U Isotope Fractionation During Coprecipitation with Aragonite and Calcite

by

Xinming Chen

A Thesis Presented in Partial Fulfillment
of the Requirements for the Degree
Master of Science

Approved April 2015 by the
Graduate Supervisory Committee:

Ariel Anbar, Chair
Pierre Herckes
Everett Shock

ARIZONA STATE UNIVERSITY

August 2015

ABSTRACT

Natural variations in $^{238}U/^{235}U$ of marine carbonates might provide a useful way of constraining redox conditions of ancient environments. In order to evaluate the reliability of this proxy, we conducted aragonite and calcite coprecipitation experiments at pH ~7.5 and ~ 8.5 to study possible U isotope fractionation during incorporation into these minerals.

Small but significant U isotope fractionation was observed in aragonite experiments at pH ~ 8.5, with heavier U in the solid phase. $^{238}U/^{235}U$ of dissolved U in these experiments can be fit by Rayleigh fractionation curves with fractionation factors of 1.00007+0.00002/-0.00003, 1.00005 ± 0.00001, and 1.00003 ± 0.00001. In contrast, no resolvable U isotope fractionation was observed in an aragonite experiment at pH ~7.5 or in calcite experiments at either pH. Equilibrium isotope fractionation among different aqueous U species is the most likely explanation for these findings. Certain charged U species are preferentially incorporated into calcium carbonate relative to the uncharged U species $Ca_2UO_2(CO_3)_3(aq)$, which we hypothesize has a lighter equilibrium U isotope composition than most of the charged species. According to this hypothesis, the magnitude of U isotope fractionation should scale with the fraction of dissolved U that is present as $Ca_2UO_2(CO_3)_3$ (aq). This expectation is confirmed by equilibrium speciation modeling of our experiments. Theoretical calculation of the U isotope fractionation factors between different U species could further test this hypothesis and our proposed fractionation mechanism.

These findings suggest that U isotope variations in ancient carbonates could be controlled by changes in the aqueous speciation of seawater U, particularly changes in seawater pH, P_{CO2}, [Ca], or [Mg] concentrations. In general, these effects are likely to be small (<0.13 ‰), but are nevertheless potentially significant because of the small natural range of variation of $^{238}U/^{235}U$.

ACKNOWLEDGMENTS

Without the help of many people, this dissertation would not have been possible. I would like to thank my advisory committee, especially Ariel Anbar and Stephen Romaniello, who supported all aspects of my research. Thank you for all your help.

I would also like to thank everyone working in the Keck Lab. In particular, Gwyneth Gordon helped me with trace metal concentration and isotopes analysis. The entire lab group is willing to help out whenever needed. I would like to appreciate the support from my family and friends. My parents offer financial support for my education and great mental help in my life and study. Thank you for my friends.

Finally, thank you for everyone who helps me.

TABLE OF CONTENTS

Page

CHAPTER PAGE

LIST OF TABLES

Table Page

LIST OF FIGURES

CHAPTER 1 INTRODUCTION

Environmental redox conditions strongly affect the oxidation states and speciation of elements, and hence element cycling and bioavailability (Anbar and Knoll, 2002; Scott et al., 2008, 2011). Biological extinctions and radiations correlate with changes in the amount of O_2 in the atmosphere and ocean (e.g., Berner et al., 2007; Canfield et al., 2007; Lyons et al., 2014; Lenton et al., 2014). Thus, tracking redox change is critical to understand the co-evolution of life and Earth.

It is difficult to reconstruct a continuous and global record of Earth's environmental redox history because the distributions of key lithologies in the geologic record are spatially and temporally sporadic. These lithologies include iron formations, phosphorites, and black shales. Frequently used paleoredox proxies in these lithologies include the abundances of redox sensitive elements (e.g., Cu, Cr, V, Cd, Mo, Y, U, Zn; Algeo and Maynard, 2004; Tribovillard et al., 2006; Algeo and Rowe, 2011) and variations in particular isotopic compositions (e.g., $\delta^{56}Fe$, $\delta^{53}Cr$, $\delta^{97/95}Mo$, $\delta^{98/95}Mo$, $\delta^{34}S$, $\Delta^{33}S$;Pufahl et al., 2012; Lyons et al., 2009; Asael et al., 2013). Unfortunately, iron formations are only common in the Paleoarchean and Paleoproterozoic, while phosphorites formed almost exclusively in the Phanerozoic (Pufahl et al., 2012). Black shales are distributed irregularly across the geological record, and were often formed in restricted marginal basins that may not represent the global marine environment (Herrmann et al., 2012).

In contrast to these lithologies, the distribution of carbonate sedimentary rocks is more continuous both temporally and spatially. The oldest preserved carbonate rocks on Earth were deposited at ~3.8 Ga (Shields and Veizer, 2002). The abundance of carbonate

rocks increases to ~20 volume % of all sedimentary rocks during the early Proterozoic (Ronov,1964) and persists at this percentage or higher throughout the Phanerozoic (Wilkinson and Walker, 1989). Therefore, it would be extremely useful to develop a reliable paleoredox proxy that can be applied to carbonate sedimentary rocks.

Rare earth elements (REEs) in carbonate rocks have been used as paleo-redox proxies for many years (German and Elderfield, 1990). In particular, the anomalous redox-sensitive behavior of Cerium (Ce) compared to the other REE in the marine environment makes it useful as a paleoredox proxy (Kakuwa and Matsumoto, 2006). However, the residence time of Ce (50 - 130 yr) is short relative to the oceanic mixing time (~10^3 yr; Jenkins, 2013), so Ce can only provide information about local redox conditions (Alibo and Nozaki, 1999; Li et al., 2013). The redox sensitive element iodine, with a long residence time of ~ 3×10^5 yr, I/Ca in marine carbonate rocks is effective for inferring the global redox conditions of ancient oceans (Lu et al., 2010; Hardisty et al., 2014; Zhou et al., 2015).

U concentrations and isotope compositions in carbonate rocks could be a very useful paleoredox proxy because oxidized U(VI) is readily incorporated into calcium carbonate mineral structures during carbonate precipitation(i.e., “coprecipitation”) in relatively high concentrations of 0.1 to 10 ppm (Chung and Swart, 1990; Kelly et al., 2003, 2006; Reeder et al., 2000). Additionally, the long residence time of U (>10^5yr; Dunk et al., 2002) suggests that, unlike Ce, U might provide globally integrated paleoredox information.

U concentrations and the U/Th ratios in sedimentary rocks have been widely used as paleoredox proxies (Anderson et al., 1989; Moford and Emerson, 1999; Wignall and

Twitchett, 1996). Under oxic conditions, U exists as soluble U(VI) in the form of uranyl carbonate complexes (Langmuir, 1978). In anoxic marine settings, U(VI) is reduced to insoluble U(IV), and subsequently adsorbed or precipitated as UO_2(s), U_3O_7 or U_3O_8 in the anoxic sediments (Klinkhammer and Palmer, 1991; McManus et al., 2005). Thus, variations of U concentrations in anoxic facies like black shales can reflect changes in redox conditions (Algeo and Maynard, 2004; Tribovillard et al., 2012). Since Th is only present as relatively insoluble Th(IV) in seawater, there is no authigenic uptake of Th under changing redox conditions. Hence, the variation of U/Th ratio in the sediments is also used as a redox proxy.

Uranium isotopes are being actively explored and applied as an additional source of ocean paleoredox information (Montoya-Pino et al., 2010; Brennecka et al., 2010, 2011a; Andersen et al., 2014; Dahl et al., 2014; Kendall et al., 2013). Natural variations in $^{238}U/^{235}U$ are known to be sensitive to redox changes (Stirling et al., 2007; Weyer et al., 2008). Low-temperature redox reactions of U are the primary drivers of U isotope fractionation on Earth, with ^{238}U preferentially enriched in reduced species (Stirling et al., 2007; Weyer et al., 2008). In the oceans, widespread anoxia causes more U to be scavenged by anoxic sediments, preferentially pulling ^{238}U from seawater and leading to a corresponding shift of $^{238}U/^{235}U$ in seawater. Because of the long residence time of U, it has been proposed that U isotope variations can be used to infer changes in global redox conditions (Weyer et al., 2008). For example, variations of $^{238}U/^{235}U$ and U concentration in black shales were used to quantify the spatial extent of marine anoxia during Oceanic Anoxic Event 2 (Montoya-Pino et al., 2010) and indicate oxidative U mobilization at 2.50 Ga (Kendall et al., 2013).

$^{238}U/^{235}U$ in modern carbonate samples is close to that of seawater (Weyer et al., 2008; Romaniello et al., 2013), suggesting that marine carbonates captures the $^{238}U/^{235}U$ of coexisting seawater. In an application of this proposed proxy, variations of $^{238}U/^{235}U$ and U/Th in a carbonate section at Dawen in southern China were interpreted as reflecting an enhancement of oceanic anoxia immediately before the end-Permian mass extinction (Brennecka et al., 2011a).

Although no resolvable U isotopic fractionation has been observed between modern aragonite and calcite samples and seawater (Weyer et al., 2008; Romaniello et al., 2013), many factors that have varied in the past, including U speciation due to variation of pH and CO_3^{2-} concentration and presence of cations (Ca^{2+}, Mg^{2+}, and Sr^{2+}), and different polymorphs of $CaCO_3$ (i.e., aragonite vs. calcite), might have caused U isotope fractionation during U incorporation into carbonate rocks. In particular, variation in U speciation in solution might lead to incorporation of differentdifferent $^{238}U/^{235}U$ ratios into carbonates if aqueous species fractionate from each other and then only certain species are incorporated into the solid phase. Different polymorphs of $CaCO_3$ may record aqueous $^{238}U/^{235}U$ differently due to U coordination changes during accommodation of U in the mineral structures. Coordination changes are known to cause resolvable isotopic fractionation during adsorption of metal complexes (i.e., U, Mo, Tl, Zn and Cu) onto synthetic K-birnessite (Juillot et al., 2008; Brennecka et al., 2011b; Wasylenki et al., 2011; Nielsen et al., 2013; Little et al., 2014; Bryan et al., 2015). Previous studies found that the predominant U(VI) species in seawater, $UO_2(CO_3)_3^{4-}$, was directly incorporated as a unit into aragonite without coordination change or reduction (Reeder et al., 2000). In

contrast, coordination change of $UO_2(CO_3)_3^{4-}$ was required to allow it to fit into calcite (Reeder et al., 2000). Hence, a difference in isotope fractionation is possible.

Here, U(VI) coprecipitation experiments with aragonite and calcite were conducted to test whether U in these two calcium carbonate polymorphs can capture the U isotope composition of seawater and thus be used as a reliable paleoredox proxy. Coprecipitation experiments were conducted at two different ocean-like pHs (~7.5 and ~8.5) to investigate the effect of U speciation (induced by pH) on U isotope fractionation during U incorporation into two $CaCO_3$ polymorphs.

CHAPTER 2 MATERIALS AND METHODS

To study U isotope fractionation during U incorporation into $CaCO_3$, U(VI) coprecipitation with aragonite and calcite was studied in experiments performed at pH ~7.5 and 8.5. Aqueous samples and solid samples were collected from each individual experiment to measure U concentration and $^{238}U/^{235}U$. When each experiment was terminated, ~1 g of the bulk precipitate was collected for X-ray diffraction (XRD) analysis to identify the $CaCO_3$ polymorph. The U(VI) speciation in the aqueous solution was calculated using the software PHREEQC (Parkhurst and Appelo, 2004) to explore the relationship between pH, U speciation, and isotope fractionation.

2.1 Materials

All labware was washed using American Chemical Society (ACS) grade nitric acid (20%), hydrochloric acid (20%), and 18.2 MΩ-cm deionized water, following standard trace metal clean lab protocols (Howard and Statham, 1993). Nitric acid and hydrochloric acid used to dissolve samples and purify U for isotope analyses were Omega trace metal grade (Fisher Scientific, Lot #4114020 (HCl) and #1114010 (HNO_3)). Chemical reagents NaCl, anhydrous $MgCl_2$, Na_2CO_3, $NaHCO_3$, $CaCl_2.2H_2O$, 30% H_2O_2 (Fisher Scientific) were ACS grade. The uranyl nitrate solution used in the U coprecipitation with aragonite and calcite experiments was an ICP-MS standard (PU1KN, Ricca Chemical Company LLC, Lot #: 4101230).

2.2 Experiments

2.2.1 Experimental setup

U coprecipitation experiments with aragonite and calcite were performed using the constant addition method (Zhong et al., 1989; Reeder et al., 2000). The experimental setup is shown in Figure 1. The reactor was a 1 L Erlenmeyer flask. Prior to $CaCO_3$ precipitation, about 5 µg of U(VI) was added into the reactor. $CaCl_2$ and Na_2CO_3/$NaHCO_3$ were delivered into the reactor via a dual syringe pump (Model: NE-1600, New Era Pump Systems, Inc.) to precipitate $CaCO_3$. The solution in the reactor was well mixed with a Teflon stir bar and bubbled with air to maintain constant P_{CO2} in the aqueous solution. The pH meter was connected to a computer to record the pH in the aqueous solution every 5 minutes.

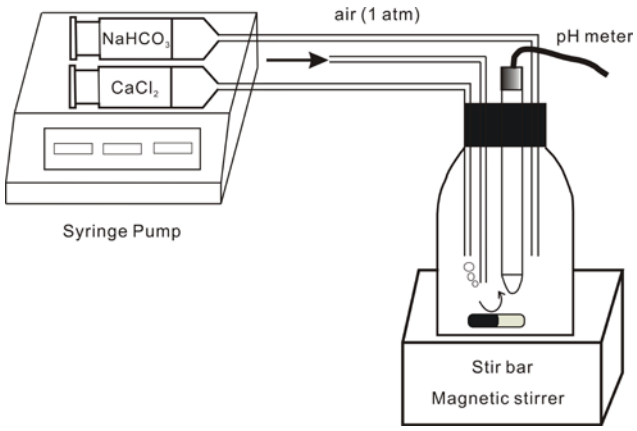

Fig. 1. Illustration of experimental setup for the constant addition method

2.2.2 U coprecipitation with aragonite and calcite procedures

Four aragonite experiments (A_1, A_2, A_3 and A_1*) and three calcite experiments (C_1, C_2 and C_3) were conducted. Aragonite experiment A_1* is the repetition of A_1. Experiments A_1, A_3, A_1*, C_1 and C_3 were conducted at pH 8.5 ± 0.1, while experiments

A_2 and C_2 were performed at pH 7.5 ± 0.1. The pH was set by adjusting the delivery rates of chemical reagents into the reactor. The experimental conditions are summarized in Table 1.

All aragonite experiments were conducted using 0.5 M $CaCl_2$ and 1.0 M $NaHCO_3$. These solutions were simultaneously delivered into the reactor through Teflon tubing (0.51 mm diameter) by a dual syringe pump equipped with two 60mL syringes. NaCl (0.5 M) was used as the background electrolyte. In aragonite experiments, a Mg^{2+}/Ca^{2+} ratio > 2 was maintained, which inhibits calcite growth by destabilizing the crystal lattice and increasing its solubility (Sanchez et al., 2009; Morse et al., 1997). To maintain a high and constant Mg^{2+}/Ca^{2+} ratio, $MgCl_2$ was added to the NaCl and $CaCl_2$ solutions. The Mg^{2+} concentration was 50 mM in experiments A_1, A_2 and A_1*, and 100 mM in experiment A_3. Prior to coprecipitation, uranyl nitrate was added into the NaCl solution to achieve an initial U concentration of ~50 μM. The high U concentration (about 3600 times that of seawater, ~ 14 nM) ensures that there is enough dissolved U for isotopic analysis of the aqueous solution even when >95% of U has been incorporated into the precipitate. Aqueous samples (~ 2 ml) were collected every 12 hours and immediately filtered through a 0.45 μm filter. Subsequently, the filtered samples were diluted with concentrated nitric acid to a final concentration of 3 M HNO_3. Part of the bulk $CaCO_3$ was dissolved with concentrated HNO_3 for U concentration and isotope ratio measurements.

The experimental conditions and procedures for calcite experiments C_1 and C_2 were the same as for aragonite experiments A_1 and A_2, except that no $MgCl_2$ was used.

The experimental procedure for calcite experiment C_3 was slightly different from the other calcite experiments. It was modified to precipitate a greater proportion of dissolved U in order to achieve a more precise measurement of the isotopic fractionation. To achieve this goal, higher concentrations of $CaCl_2$ (2.0 M) and Na_2CO_3 (2.0 M) were used. To keep ionic strength constant, 2.0 M NaCl was used as background electrolyte. One gram of calcite seed crystals were added into the NaCl solution and mixed with a stir bar for 18 hours. Subsequently, uranyl nitrate was introduced into the NaCl solution to attain a U concentration of 50 μM. During the calcite coprecipitation process, aliquots of aqueous solution (~ 2 ml) were collected every 12 hours. To compare the U isotope ratio between aqueous solution and instantaneous solid, each day a clean glass microscope slide was submerged into the solution to collect daily precipitate, to be retrieved after 24 hours. When experiment C_3 ended, bulk solid was also taken for XRD analysis. The preparation procedures for U concentration and its isotopic ratio analysis in aqueous and solid samples were the same as in all other experiments.

2.3 X-Ray Diffraction

About 1 g of the bulk precipitate from each experiment was collected, ground using an agate mortar and pestle, and loaded into a sample holder. The crystal structures of synthetic carbonates were characterized by powder XRD (Bruker-AXS D8 Advance, ASU) using Cu Kα radiation (40 kV and 30 mA) and a Ni filter with a scanning speed of 0.005° 2θ s^{-1}. The time constant was 2 seconds. The crystal structures of the synthetic calcium carbonates were verified by comparing the spectra with those of calcite and aragonite standards from the International Center for Diffraction Data.

2.4 U concentration analysis

Aqueous samples collected during U coprecipitation with aragonite and calcite were diluted to 0.32 M nitric acid for U concentration analysis using quadrupole inductively-coupled plasma mass spectrometry (ICP-MS, Thermo X series) at Arizona State University (ASU). About 0.1 g of $CaCO_3$ from each experiment was dissolved with 1 ml of 3 M HNO_3. The estimated precision for the U concentration measurements by ICP-MS was ~ ±2% based on repeated analysis of check standard solutions during the runs.

2.5 U isotope analysis

2.5.1 ^{233}U-^{236}U double spiking

The ^{233}U-^{236}U double-spike method was used to measure U isotope ratio using multiple collector ICP-MS (MC-ICP-MS) (Weyer et al., 2008). The double spike method is the most effective way to correct for instrumental mass bias and potential isotope fractionation during U purification (Rudge et al., 2009). About 500 ng of U from each sample was well mixed with a sufficient double-spike U solution IRMM 3636 U to achieve a $(^{233}U)_{spike}/(^{235}U)_{sample}$ ratio of ~ 2.5 (Verbruggen et al., 2008). The samples were spiked prior to chromatographic separation to correct for any U isotope fractionation that might occur during U purification.

2.5.2 U purification

U purification was carried out following the protocol of Weyer et al. (2008). The column was first rinsed with 10 ml 18.2 MΩ-cm deionized water. A volume of 0.8 ml UTEVA resin (Eichrom Technologies, LLC) was loaded on a column. The resin was then

washed with 4×2.5 ml 0.05 M HCl to remove impurities. The resin was then converted to the nitric form by loading 3×0.8 ml 3 M HNO_3. The double-spiked U sample (dissolved in 3 M HNO_3) was loaded on the column and rinsed with 5×2 ml 3 M HNO_3 to remove all matrix ions except U and Th. Then, 10 M HCl (3×0.8 ml) was added to the column to convert the UTEVA resin to chloride form. Th was removed from the resin using a mixture of 5 M HCl and 0.05 M oxalic acid (3×0.8 ml). The oxalic acid left on the resin was rinsed of with 3×0.8 ml 5 M HCl. The U adsorbed on the resin was eluted with 7 ml (1+1+1+2+2) 0.05 M HCl. The U cuts were dried down and heated with concentrated HNO_3 + 30% H_2O_2 (1 + 0.3 ml) to remove any residual organic residue eluted from the UTEVA resin. The last step was repeated until all organic residue was removed. The sample was finally dissolved in 0.32 M HNO_3 for U isotope measurement.

2.5.3 U isotopic ratio measurements on mass spectrometry

The U isotope ratios were measured at ASU using MC-ICP-MS (Thermo Scientific Neptune). Samples were dissolved in 0.32 M HNO_3 with a U concentration of ~50 ppb and introduced into the instrument via an Apex-Q desolvation introduction system. Ion beams of ^{233}U, ^{235}U, ^{236}U, and ^{238}U were collected with Faraday cups connected to 10^{12} Ω, 10^{12} Ω, 10^{12} Ω, and 10^{11} Ω resistors respectively. The typical voltage for ^{238}U of 50 ppb U was ~30 V. U isotopic compositions are reported in δ notation relative to the standard CRM-145 using the following equation:

$$\delta^{238}U=\left[\frac{\left(^{238}U/^{235}U\right)_{sample}}{\left(^{238}U/^{235}U\right)_{standard}}-1\right]\times 1000 \quad (1)$$

where $(^{238}U/^{235}U)_{sample}$ and $(^{238}U/^{235}U)_{CRM\text{-}145}$ are the U isotope ratio of a sample and the standard, respectively.

Each sample was measured at least three times. The U isotope measurement precision is reported as twice of the standard deviation (2 SD) of the replicate measurements of each individual sample. The CRM-145 standard was run every third analysis to correct for the small amounts of instrument drift. The reproducibility of replicate measurements of the U isotope composition of the standard CRM-145 is within ± 0.10 ‰ (2 SD). The accuracy of the U isotope measurement was assessed by measuring the standard CRM-129a. The measured average $\delta^{238}U$ of CRM-129a is -1.70 ± 0.08 ‰ (2 SD), which agrees with previous published values (Wang et al., 2014; Weyer et al., 2008; Shiel et al., 2013).

2.5.4 Data analysis

Experimental results were analyzed via linear regression to determine observed fractionation factors and their respective uncertainties using the ISOPLOT 3.75 software (Ludwig, 2012). ISOPLOT uses two-variable York regression, which considers the uncertainties in both the independent and dependent variables, to determine the regression parameters along with their respective uncertainties. The ISOPLOT software package is widely used in fields such as geochronology which require robust, reliable, and precise data regression. Such careful treatment of linear regression analysis is particularly important for this project as the experimentally-determined isotopic fractionation factors (α, discussed below) are relatively small compared to the errors on individual measurements. As such, it is sometimes impossible to visually inspect the data and determine a significant slope. Instead, linear regression is used to precisely determine isotopic fractionation factors from the regression slope. The errors on the slope, reported at the 2 SD (~95% confidence level), are used to determine whether the isotopic

fractionation factor is significantly different from α=1 (no fractionation). Because the precision of these linear regressions depends on the spread of the independent (x-axis) data, experiments were intentionally designed to maximize this spread by ensuring a high degree of U incorporation into the carbonate.

2.6 U speciation

The U(VI) speciation over the pH range 7 – 9 was modeled with the software PHREEQC (Parkhurst and Appelo, 2004) using database **sit**.**dat** with updated U thermodynamic data from Grenthe et al. (1992) and Guillaumont et al. (2003). The three new aqueous uranyl complexes $Ca_2UO_2(CO_3)_3(aq)$, $CaUO_2(CO_3)_3^{2-}$, and $MgUO_2(CO_3)_3^{2-}$ were added into the U speciation modeling (Dong and Brooks, 2006). Specific ion interaction theory (SIT) was employed to estimate single-ion activity coefficients at high ionic strength (0.5~2.0 M) with NaCl as the background electrolyte.

CHAPTER 3 RESULTS

3.1 U coprecipitaiton with aragonite and calcite

U coprecipitation experiments with aragonite and calcite were conducted under different conditions as shown in Table 1. The pH of these experiments increased from 7.0 to 9.5 until the first calcium carbonate nucleated on the wall the glass reactor. Subsequently, the pH dropped quickly to be relatively stable when the amount of calcium pumped into the reactor was balanced via precipitation as $CaCO_3$. The pH (8.50 and 7.50) in our experiments was controlled by adjusting delivery rates of chemical reagents into the reactor, with higher pH at slower delivery rate and vice versa.

The measured U concentrations in aragonite and calcite precipitates were about 2300 ppm and 300 ppm, respectively, and were at most only weakly dependent on pumping speed or pH （Table 1). The weak dependence of U concentrations on speed or pH might be the result of the high growth rate (Gabitov et al., 2008). More than 94% of the total U was incorporated into aragonite in experiments A_1 and A_2, whereas less than 18% of U was incorporated into calcite in experiment C_1 and C_2. In experiment C_3, approximately 90% of the total U was incorporated.

Table 1. Summary and results of $CaCO_3$ coprecipitation experiments

Experiments	pH	Electrolyte NaCl (M)	Reagents	Pumping rate (μl/min)	Time (hrs)	Mg^{2+} (mM)	Ca^{2+} (mM)	$CaCO_3$ (g)	U uptake (%)	$[U/CaCO_3]_{solid}$ (ppm)
A_1	8.50±0.10	0.50	$CaCl_2$+$NaHCO_3$	4	160	50	5	1.94	94.9	2145
A_2	7.50±0.10	0.50	$CaCl_2$+$NaHCO_3$	40	16	50	5	1.71	98.6	2525
A_3	8.50±0.10	0.50	$CaCl_2$+$NaHCO_3$	4	160	100	4	1.96	98.2	2075
A_1*	8.50±0.10	0.50	$CaCl_2$+$NaHCO_3$	4	160	50	4.8	1.95	93. 7	2053
C_1	8.50±0.10	0.50	$CaCl_2$+$NaHCO_3$	4	160	0	2	1.91	14.5	336
C_2	7.50±0.10	0.50	$CaCl_2$+ $NaHCO_3$	40	16	0	2	1.64	17.5	360
C_3	8.50±0.10	2.00	$CaCl_2$+Na_2CO_3	10	168	0	3.5	19.44	90.5	250

3.2 XRD analysis

The XRD spectra of the synthetic carbonates (C_1, C_2, C_3, A_1 and A_2) were compared to those of a calcite standard (R040070) and an aragonite standard (R040078). As shown in Fig. 2, spectra of synthetic carbonates matched perfectly with their corresponding standards. Although no XRD analysis was done for precipitates in experiments A_3 and A_1*, the higher Mg^{2+}/Ca^{2+} ratios in these experiments (> 10) relative to that in aragonite experiment A_1 (~9) indicate that the polymorph of $CaCO_3$ in A_3 and A_1^* should also be aragonite (Sanchez et al., 2009; Morse et al., 1997).

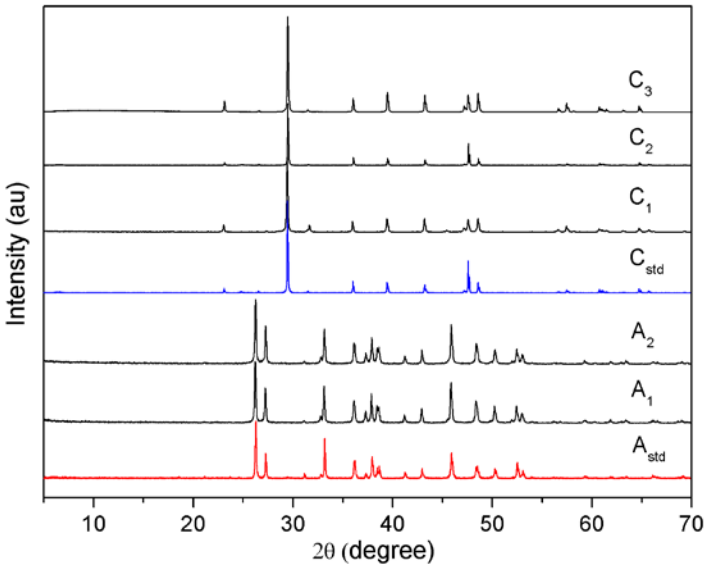

Fig. 2. XRD spectra of calcium carbonate. A_1 (aragonite 1), A_2 (aragonite 2), A_{std} (aragonite standard), C_1 (calcite 1), C_2 (calcite 2), C_3 (calcite 3), C_{std} (calcite standard).

3.3 U speciation

The U(VI) speciations over the pH range of 7 – 9 at different experimental conditions are displayed in Fig. 3. U speciation varies significantly at pH 8.50 and 7.50 in all calcite and aragonite experiments. U speciation also varies between aragonite and calcite experiments (Fig. 3a vs. Fig. 3c) due to the presence of Mg-U species ($MgUO_2(CO_3)_3^{2-}$) in the aragonite experiments.

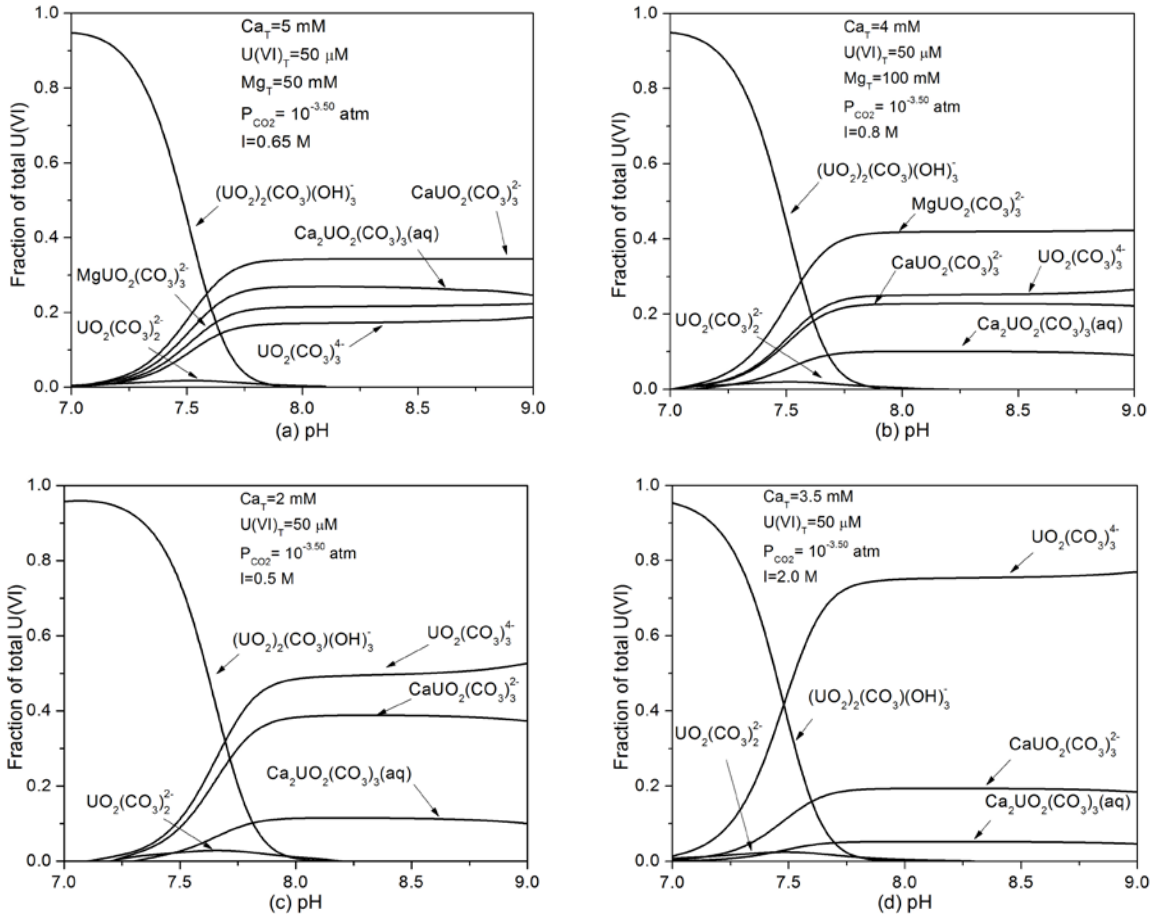

Fig. 3. Aqueous U(VI) speciation as a function of pH (7-9) for aragonite and calcite experiments at $P_{CO2} = 10^{-3.5}$ atm. (a) U(VI) speciation in aragonite experiments A_1, A_2 and A_1* with ionic strength I=0.65 M, total Ca^{2+} concentration 5 mM, Mg^{2+} concentration 50 mM, U speciation in A_1* is slightly different from that in A_1 due to the lower concentration of Ca^{2+} (4.8 mM); (b) U(VI) speciation in aragonite experiment A_3 with ionic strength I=0.8 M, total Ca^{2+} concentration 4 mM, Mg^{2+} concentration 100 mM; (c) U(VI) calcite experiments C_1 and C_2 with ionic strength I=0.5 M, total Ca^{2+} concentration 2 mM; (d) U(VI) speciation in calcite experiment C_3 with ionic strength I=2.0 M, total Ca^{2+} concentration 3.5 mM.

U speciation is dominated by $CaUO_2(CO_3)_3^{2-}$ (~33%) in experiments and A_1 and A_1* at pH 8.50 (Fig. 3a). However, in experiment A_2, conducted at lower pH (7.50 vs. 8.50), $(UO_2)_2(CO_3)(OH)_3^-$ (50%) is the dominant U species. When the Mg^{2+} concentration in experiment A_3 is about twice of that in experiments A_1 and A_1*, $MgUO_2(CO_3)_3^{2-}$ become the dominant U species, accounting for 42% of the total U species at pH 8.50.

Fig. 3c shows that $UO_2(CO_3)_3^{4-}$ (50%) is the predominant U species in experiment C_1 at pH 8.50, and that $(UO_2)_2(CO_3)(OH)_3^-$ (~55%) becomes another important U species in experiment C_2 at lower pH (7.50). In experiment C_3 (Fig. 3d), $UO_2(CO_3)_3^{4-}$ (75%) is the dominant U species. Although the U concentration in the solution decreased during the course of these carbonate coprecipitation experiments, our modeling shows that U speciation stayed the same (not shown here).

3.4 U isotope fractionation in aragonite and calcite experiments

3.4.1 Aragonite experiments

U isotopic compositions in the aqueous and bulk solid samples in aragonite coprecipitation experiments are displayed in Fig. 4. Based on repeated analysis, the starting stock (ICP standard Ricca) has a $\delta^{238}U$ of -0.23 ± 0.06 ‰ (2 SD, N=28). Thus, U isotopic compositions at the beginning of aragonite and calcite coprecipitation experiments are -0.23 ± 0.06 ‰. To verify mass balance, we compared $\delta^{238}U$ in the bulk aragonite at the end of the experiments, when > 94% of the U in the solution was incorporated into the aragonite, to that of the initial solution. These values are identical to

the starting stock within the uncertainties (A_1: -0.22 ± 0.08 ‰, A_1*: -0.23 ± 0.02 ‰, A_2: -0.30 ± 0.05 ‰, and A_3: -0.29 ± 0.07 ‰), consistent with expectations.

To estimate the magnitude of the U isotope fractionation factor in experiments, the data in each experiment were fitted using the Rayleigh fractionation model, which assumes that coprecipitated U was continuously incorporated into the solid phase and isolated from further isotope exchange with the aqueous solution. The instantaneous isotope fractionation factor, α, is defined as:

$$\alpha = \frac{\left({}^{238}\mathrm{U}/{}^{235}\mathrm{U} \right)_{\mathrm{solid}}}{\left({}^{238}\mathrm{U}/{}^{235}\mathrm{U} \right)_{\mathrm{solution}}} \quad (2)$$

where $({}^{238}\mathrm{U}/{}^{235}\mathrm{U})_{\mathrm{solid}}$ and $({}^{238}\mathrm{U}/{}^{235}\mathrm{U})_{\mathrm{solution}}$ are the isotopic ratios of U incorporated into the solid at an instant in time and that in the remaining solution, respectively. If the isotopic fractionation factor is significantly different from 1, there is isotopic fractionation between U in the aqueous solution and instantaneous solid. The value of α was determined by linear fitting to the following equation:

$$\ln\left(\delta^{238}\mathrm{U}_{\mathrm{solution}} + 1000\right) = (\alpha - 1)\ln f + \ln\left(\delta^{238}\mathrm{U}_0 + 1000\right) \quad (3)$$

where $\delta^{238}\mathrm{U}_{\mathrm{solution}}$ and $\delta^{238}\mathrm{U}_0$ (-0.23 ± 0.06 ‰) are the U isotopic compositions of the solution at the time of sampling and at the beginning of the experiments, respectively, and *f* is the fraction of U remaining in the aqueous solution (Mariotti et al., 1981). The uncertainty of the slope (α-1) in equation (3) is estimated using the ISOPLOT 3.75 software (Ludwig, 2012; York, 1966). Results of linear regression of all the experiments are displayed in APPENDIX C.

The U isotopic compositions in the accumulated solid were calculated using the mass balance equation:

$$\delta^{238}U_{solid} = \frac{\delta^{238}U_0 - f \times \delta^{238}U_{solution}}{1-f} \quad (4)$$

where $\delta^{238}U_{solid}$ is the U isotopic composition of the accumulated solid when a fraction of total U (1-*f*) was incorporated into the aragonite. The $\delta^{238}U_{solid}$ at the beginning of each experiment was assumed to be the $\delta^{238}U$ in the instantaneous solid.

The U isotope fractionation factors (α) derived in equation (1) for experiments A_1 A_1*, A_2 and A_3 were 1.00007 +0.00002/-0.00003, 1.00005 ± 0.00001, 1.00001 ± 0.00002, and 1.00003 ± 0.00001, respectively. All these isotopic fractionation factors are larger than 1, suggesting that heavier U isotopes will be preferentially incorporated into aragonite. Within uncertainty, the U isotope fractionation in aragonite A_1 is indistinguishable from that in A_1*.

The variations of $\delta^{238}U$ values vs. *f* in experiment A_1, A_1*, A_2 and A_3 could alternatively be fit with a linear model. However, the respective regression coefficients (R^2) for A_1, A_1*, A_2 and A_3, 0.69 and 0.76, 0.35 and 0.60, are lower than those derived from the Rayleigh fractionation model (0.89, 0.89, 0.56 and 0.90). Thus, the Rayleigh model is a better fit.

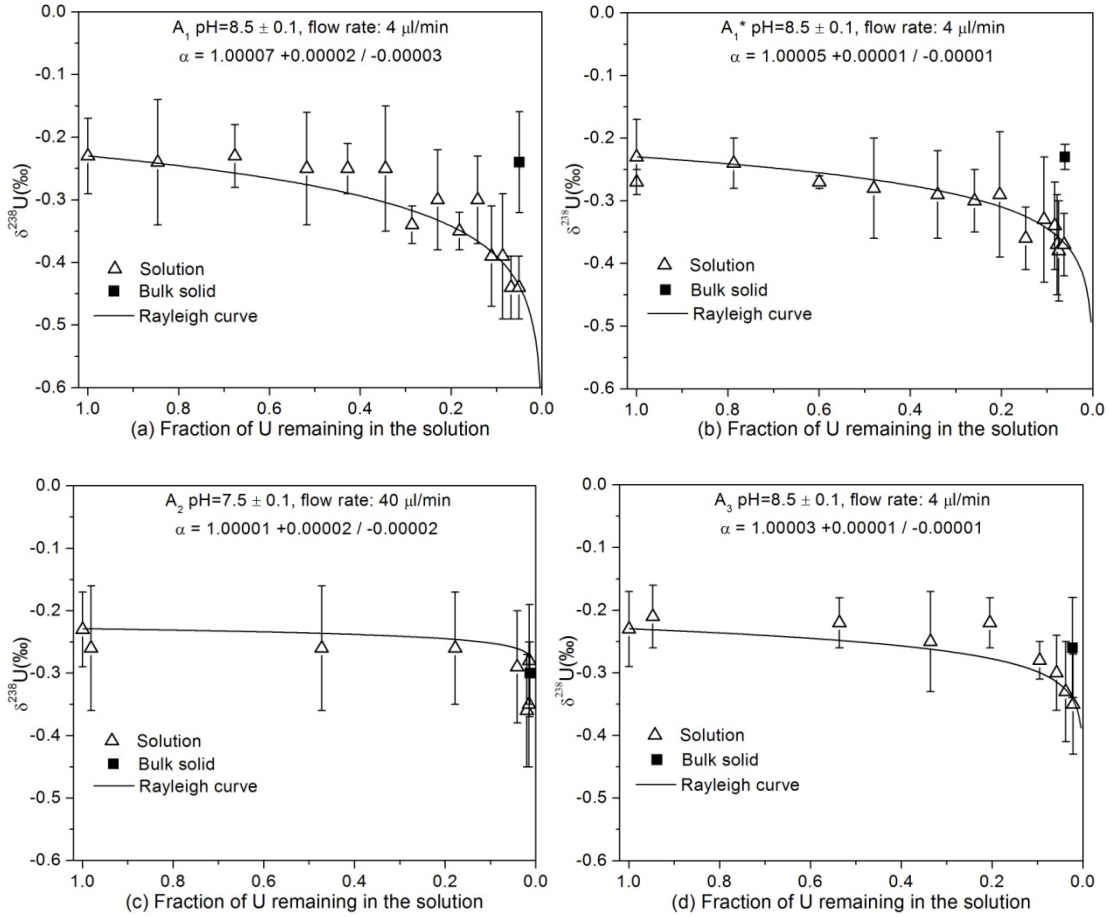

Fig. 4. U isotopic compositions of the aqueous and solid samples versus fraction of U remaining in the aqueous solution for aragonite experiments A_1, A_1*, A_2 and A_3. The open triangles and filled rectangles represent the U isotopic compositions of aqueous samples and bulk solid samples, respectively. The black curves are Rayleigh fractionation curves.

3.4.2 Calcite experiments

U isotopic compositions of the aqueous, daily solid and bulk solid samples in calcite experiments are depicted in Fig. 5. The U isotopic data in calcite coprecipitation experiments were also fitted using Rayleigh fractionation model. All the Rayleigh fractionation factors are summarized in Table 2.

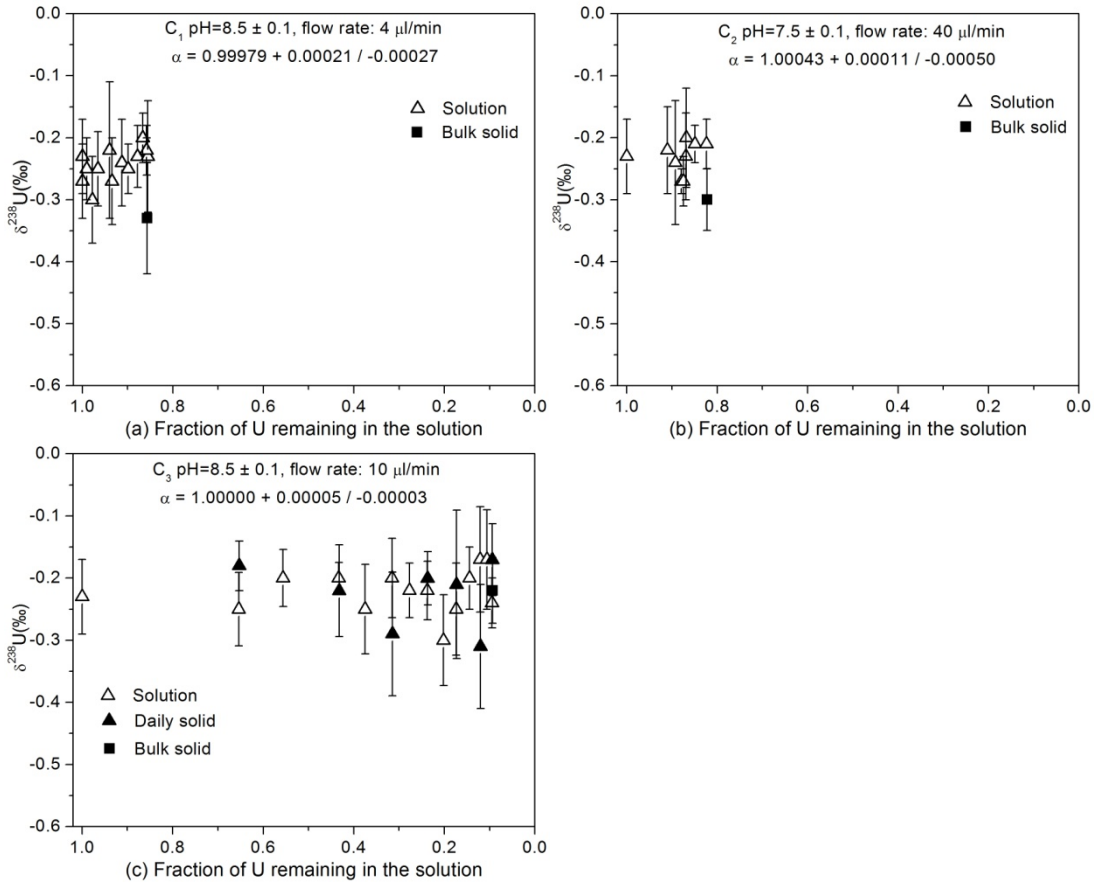

Fig. 5. U isotopic composition in aqueous and solid samples versus fraction of U incorporated into calcite. The open triangles, filled triangles and filled rectangles are the U isotopic compositions of aqueous samples, daily solid samples and bulk solid samples, respectively.

The Rayleigh fractionation factors in calcite experiments C_1 (0.99979 +0.00021/-0.00027) and C_2 (1.00043 +0.00011/-0.00050) have large uncertainties due to limited degree of U incorporation (<18%, Fig. 5a and Fig. 5b). The small degree of U incorporation leads to a narrow range of *f* in equation (3), resulting in large slopes (α-1) of the lines and big uncertainties in the slopes during linear fitting. The Rayleigh isotopic

fractionation factors in C_1 and C_2 are statistically indistinguishable from 1, suggesting that there is no resolvable U isotopic fractionation during U coprecipitation with calcite.

The Rayleigh isotopic fractionation factor of 1.00000 +0.00005/-0.00003 in C_3 at pH 8.50 also suggests that there is no resolvable U isotopic fractionation during calcite precipitation. This is consistent with the unresolvable U isotopic fractionation between aqueous samples and daily solid samples in Fig. 5c. The higher degree of U uptake in C_3 (90.5%) reduces the uncertainty in the estimation of Rayleigh fractionation factor.

Table 2. Rayleigh isotopic fractionation factors in aragonite and calcite experiments

Experiments	pH	U uptake (%)	$f_{neutral}$	Rayleigh isotopic fractionation factor (α)
A_1	8.50 ± 0.10	94.9	0.27	1.00007 +0.00002/-0.00003
A_1*	8.50 ± 0.10	93.7	0.24	1.00005 +0.00001/-0.00001
A_2	7.50 ± 0.10	98.6	0.13	1.00001 +0.00002/-0.00002
A_3	8.50 ± 0.10	98.2	0.09	1.00003 +0.00001/-0.00001
C_1	8.50 ± 0.10	14.5	0.11	0.99979 +0.00021/-0.00027
C_2	7.50 ± 0.10	17.5	0.05	1.00043 +0.00011/-0.00050
C_3	8.50 ± 0.10	90.5	0.05	1.00000 +0.00005/-0.00003

Note: $f_{neutral}$ is the fraction of neutral U species $Ca_2UO_2(CO_3)_3(aq)$.

CHAPTER 4 DISCUSSION

The experimental results revealed a small U isotopic fractionation in aragonite coprecipitation experiments at pH 8.50. However, no resolvable U isotopic fractionation was observed in aragonite experiment at pH 7.50 or calcite experiments. Below we discuss possible explanations for these experimental results.

4.1 U isotope fractionation mechanism

The direction of the fractionation seen in most of the aragonite experiments – favoring incorporation of heavy U isotopes into aragonite – contradicts a simple kinetic isotope fractionation model, which would result in preferential incorporation of light U isotopes into the solid phase. The most important driver of isotopic fractionation for the heavy element U is the nuclear volume effect, which leads to preferential enrichment of heavy U isotopes in U(IV) during U(VI) reduction (Bigeleisen 1996; Schauble, 2007; Brennecka et al., 2010; Basu, 2013; Bopp et a., 2009, 2010). However, in our experiments, U is always in the (VI) oxidation state. As a result, the most likely driver of isotopic fractionation in these experiments is equilibrium isotopic fractionation driven by changes in chemical speciation in solution or during the co-precipitation process.

Below we consider two possible drivers of the observed effect: change in U speciation *during* incorporation of U into the solid phase; and speciation differences among various aqueous U(VI) species *prior* to incorporation. In both cases, isotopes may partition differentially among the species with different chemical bonding environments.

4.1.1 Change in U speciation during incorporation into $CaCO_3$

Change in U speciation during incorporation of U into the solid phase might be one mechanism driving U isotope fractionation in our experiments. It has been observed that coordination changes of Mo, U, Tl, Cu and Zn during adsorption onto Mn-oxyhydroxides led to resolvable isotopic fractionation (Barling et al., 2004; Wasylenki et al., 2011; Brennecka et al., 2011b; Nielsen et al., 2013; Little et al., 2014). Generally, metal complexes with smaller coordination number and shorter bond length have stronger chemical bonds, favoring incorporation of heavier isotopes (Schauble et al., 2004).

However, we think this mechanism cannot explain our results. Previous studies found that the predominant U(VI) species $UO_2(CO_3)_3^{4-}$ in aqueous solution at pH >8.2 was incorporated wholesale into aragonite without a change in U coordination (Reeder et al., 2000). In contrast, the coordination number and bond length both decrease during $UO_2(CO_3)_3^{4-}$ incorporation into calcite (Reeder et al., 2000). Thus, if coordination change upon incorporation to the mineral causes resolvable isotope fractionation, it is reasonable to expect that heavier U isotopes will be preferentially incorporated into calcite, and that no U isotopic fractionation will be observed in aragonite. If the U isotopic fractionation driven by coordination change is too small to be resolved, no U isotopic fractionation should be observed in either the aragonite and calcite experiments. Since our data do not conform to either expectation, our results are not consistent with coordination change as the driver of the observed fractionation.

4.1.2 Differences in aqueous U speciation prior to incorporation

Differences in aqueous U speciation prior to incorporation might be another mechanism driving the U isotope fractionation. U speciation changes significantly with pH. Our speciation calculations indicate that the distribution of U species was not the same in our experiments at pH 7.50 and 8.50. In aragonite experiment A_1, A_1*, and A_3, at pH 8.50, four U(VI) species $CaUO_2(CO_3)_3^{2-}$, $MgUO_2(CO_3)_3^{2-}$, $Ca_2UO_2(CO_3)_3$(aq), and $UO_2(CO_3)_3^{4-}$ should be present in significant amounts (Fig. 3a). However, in calcite experiments C_1 and C_3, at pH 8.50, only three U species $UO_2(CO_3)_3^{4-}$, $Ca_2UO_2(CO_3)_3$(aq) and $CaUO_2(CO_3)_3^{2-}$ should coexist. Finally, in experiments A_2 and C_2 at pH 7.50, we expect that $(UO_2)_2(CO_3)(OH)_3^-$ became the dominant U species.

Isotopic fractionation of U between different aqueous species is controlled by the local chemical bonding environments, including the coordination number and bond length (Schauble et al., 2004). The coordination number of equatorial O atoms, and bond lengths between U and axial O, and between U and equatorial O of these U species, are shown in Table 3. Differences in coordination and bond lengths suggest that there may be significant isotopic fractionation between various species. Table 3 organizes U species with similar bonding environments into several groups. For example, Group 1, containing $UO_2(CO_3)_3^{4-}$ and $Ca_2UO_2(CO_3)_3$(aq), shares a similar 6-fold coordination, with axial bond length ($U\text{-}O_{ax}$) of 1.80 Å and equatorial bond lengths ($U\text{-}O_{eq}$) of 2.43 ± 0.01 Å. Because of the similarity in chemical bonding environments, these species are expected to have similar U isotopic fractionation. Group 2, containing $CaUO_2(CO_3)_3^{2-}$ and $MgUO_2(CO_3)_3^{2-}$, differs in that the equatorial bond lengths are 2.39 ± 0.01 Å. Group 3 [$UO_2(CO_3)_2^{2-}$] and Group 4 [$(UO_2)_2(CO_3)(OH)_3^-$] contains the remaining species, which have variable

bonding environments, but which are only major U species below pH < 8.0. Because these groups have different chemical bonding environments, it is reasonable to expect U isotope fractionation between these groups.

Theoretical calculations and lab experiments have demonstrated the qualitative rule that chemical species with lower coordination number and shorter bond length, generally, favors heavier isotopes of an element (Schauble et al., 2004; Zeebe, 2004; Bogatko et al., 2013; Colla et al., 2013; Fujii et al., 2013; Huang et al., 2014). B isotope fractionation as large as 19.1 ‰ was estimated between threefold coordinated $B(OH)_3$ and fourfold coordinated $B(OH)_4^-$, with heavier B isotopes enriched in $B(OH)_3$ (Zeebe, 2004). Enrichment of heavier isotopes was also found in cations like Li^+, Mg^{2+}, Ca^{2+}, and Cu^{2+} with lower coordination number of H_2O molecules and shorter metal-O bond length (Bogatko et al., 2013; Kowalski and Jahn, 2011; Colla et al., 2013; Fujii et al., 2013; Huang et al., 2014). Quantum chemical methods demonstrate that the carbonate ligand (CO_3^{2-}) offers a stronger chemical bonding environment for uranyl (VI) complexes relative to hydroxide ligand (OH^-) (Vallet et a., 2012). Based on these qualitative rules, it is reasonable to predict that U species of Group 1 ($Ca_2UO_2(CO_3)_3(aq)$ and $UO_2(CO_3)_3^{4-}$) might be the isotopically lightest, because they have the longest U-O_{eq} bond lengths (identical in both species to within the ± 0.01 Å uncertainty of these data), the highest coordination number, and no OH^- ligands.

Table 3. Coordination numbers and distances between U and its nearest atoms

	U(VI) species	Coordination number ($U\text{-}O_{eq}$)	$U\text{-}O_{ax}$ (Å)	$U\text{-}O_{eq}$(Å)	References
Group 1	$UO_2(CO_3)_3^{4-}$	6.0	1.80	2.43	Docrat et al., 1999
	$Ca_2UO_2(CO_3)_3$(aq)	6.0	1.80	2.44	Bernhard et al., 2001
Group 2	$CaUO_2(CO_3)_3^{2-}$	6.0	1.80	2.40	Kerisit et al., 2010
	$MgUO_2(CO_3)_3^{2-}$	6.0	1.80	2.39	Kerisit et al., 2010
Group 3	$UO_2(CO_3)_2^{2-}$	4.0	1.81	2.36	Kerisit et al., 2010
Group 4	$(UO_2)_2(CO_3)(OH)_3^-$	1.3	1.80	2.36	Szabo et al., 2000
		3.9		2.45	
Calcite Bonding Environment	Adsorbed-U on calcite (pH=8.3)	6.0	1.80	2.40	Elzinga et al., 2004
	Adsorbed-U on calcite (pH=7.4)	3.0	1.80	2.25	Elzinga et al., 2004
		3.0		2.45	

Note: $U\text{-}O_{ax}$ is the distance between U and axial O; $U\text{-}O_{eq}$ is the distance between U and equatorial O. The uncertainty for the measurements the bond length is within ± 0.01 Å.

How might such a difference in isotope composition among the dissolved species explain the difference in isotopic fractionation factors observed in these experiments? We hypothesize a scenario based on the different affinities of charged vs. uncharged U(VI) species for mineral surfaces. These differences are well known. For example, U(VI) adsorption to ferrihydrite and quartz decreased significantly when the fraction of the neutral U species $Ca_2UO_2(CO_3)_3$(aq) increased in the aqueous solution (Fox et al., 2006; Bernhard et al., 2001). Of relevance here, the presence of calcite in soils and subsurface sediments was found to significantly suppress U(VI) sorption onto $CaCO_3$ and soils because of the formation of neutral uranyl complex $Ca_2UO_2(CO_3)_3$(aq) (Zheng et al., 2003; Dong et al., 2005). This neutral species should have a lower affinity for $CaCO_3$ surfaces than do anionic species because these surfaces are positively charged at pH < 10.0 (Tunusoglu, 2007). Consistent with this expectation, spectroscopic investigation of U(VI) sorption at the calcite-water interface shows that the U-O bond lengths of the U

species adsorbed onto calcite are similar to those of $CaUO_2(CO_3)_3^{2-}$ at pH 8.3 (Elzinga et al., 2004). Thus, it is reasonable to assume that in our experiments the charged U species in the aqueous solution are preferentially incorporated into aragonite and calcite relative to the neutral U species $Ca_2UO_2(CO_3)_3(aq)$.

If we assume that only the charged species are incorporated into the mineral, and make the simplifying assumption that these species are all incorporated to the same extent as each other, then the isotopic composition of U incorporated into the solid at any instant (the "instantaneous solid") will be the same as the average isotopic composition of all charged U species in the aqueous solution. In this scenario, isotope fractionation between dissolved and mineral-bound U occurs because $Ca_2UO_2(CO_3)_3(aq)$, which has the lightest $\delta^{238}U$, is not incorporated into the mineral. As a consequence, the isotope fractionation between the U in the aqueous solution and U incorporated into the mineral should increase as the relative abundance of $Ca_2UO_2(CO_3)_3(aq)$ vs. the charged U species increases.

4.1.3 Quantitative modeling of U isotopic variations due to changes in aqueous U speciation

Section 4.1.2 proposes a qualitative model for how variations in the abundance of charged and uncharged U species could affect isotopic fractionation of U during incorporation into calcite and aragonite. The goal of this section is to construct a quantitative model of this process and use this model to predict isotopic fractionation as a function of the abundance of neutrally charged U species.

Because the isotopic fractionation between different aqueous U species is not known experimentally and is difficult to accurately simulate using quantum mechanical approaches, the modeling approach described below takes advantage of groupings of similar bond strengths in Table 2 and mass balance calculations to determine the relative isotopic fractionations between aqueous U species.

The basic hypothesis put forth in Section 4.1.2 is that the isotopic composition of U incorporated into the instantaneous calcium carbonate ($\delta^{238}U_{instantaneous}$) is equal to the abundance-weighted average isotopic composition of charged U species in solution ($\delta^{238}U_{charged}$). It follows that the experimentally determined U isotopic fractionation factor (α) during coprecipitation experiments reflects the difference between $\delta^{238}U_{charged}$ and the average composition of total dissolved aqueous U species ($\delta^{238}U_{total}$):

$$(\alpha\text{-}1) \times 1000 \approx \delta^{238}U_{instantaneous} - \delta^{238}U_{total} = \delta^{238}U_{charged} - \delta^{238}U_{total} \quad (5)$$

The isotopic composition of the charged species is related to the isotopic composition of the total dissolved U species via an isotopic mass balance equation involving the charged ($\delta^{238}U_{charged}$) and uncharged U ($\delta^{238}U_{neutral}$) species:

$$f_{neutral} \times \delta^{238}U_{neutral} + (1 - f_{neutral}) \times \delta^{238}U_{charged} = \delta^{238}U_{total} \quad (6)$$

where $f_{neutral}$ is the molar fraction of neutrally-charged U species - $Ca_2UO_2(CO_3)_3(aq)$ - in aqueous solution.

Because equation (6) contains two unknowns ($\delta^{238}U_{neutral}$, $\delta^{238}U_{charged}$) we cannot solve it without a second isotopic mass balance equation. For the pH = 8.50 experiments, the aqueous U speciation is dominated by four U species representing >99.99% of total dissolved U. These four species can be grouped into two groups (Group 1 and 2 in Table

2) based on similarities in their local bonding environments, and thus the isotopic composition of U species within each group should be identical. Based on these grouping, a second isotopic mass balance experiment can be written:

$$f_1 \times \delta^{238}U_1 + (1-f_1) \times (\delta^{238}U_1 + \Delta^{238}U_{2\text{-}1}) = \delta^{238}U_{total} \quad (7)$$

where f_1 is the fraction of group 1. $\delta^{238}U_1$ stands for the U isotope composition of group 1. $\Delta^{238}U_{2\text{-}1}$ is the $\delta^{238}U$ difference between the two groups of U species due to the equilibrium isotope fractionation. Because the neutral U species $Ca_2UO_2(CO_3)_3(aq)$ is a member of group 1, $\delta^{238}U_{neutral}$ is equal to $\delta^{238}U_1$. Using this information, the difference of isotopic compositions between neutral U species and total dissolved U species ($\Delta^{238}U_{neutral\text{-}total}$) can be derived from equation (7). A step-by-step derivation of equation (8) is provided in Appendix A.

$$\begin{aligned}\Delta^{238}U_{neutral\text{-}total} &= \delta^{238}U_{total} - \delta^{238}U_{neutral} \\ &= (f_1 - 1)\Delta^{238}U_{2\text{-}1}\end{aligned} \quad (8)$$

Combing equations (5) and (6), the difference of isotopic compositions between neutral U species and total dissolved U species ($\Delta^{238}U_{neutral\text{-}total}$) can also be written as

$$\begin{aligned}\Delta^{238}U_{neutral\text{-}total} &= \delta^{238}U_{neutral} - \delta^{238}U_{total} \\ &= \frac{f_{neutral} - 1}{f_{neutral}}(\alpha - 1) \times 1000\end{aligned} \quad (9)$$

From equations (8) and (9), the U isotopic fractionation factor (α) can be derived as

$$\alpha = \frac{\Delta^{238}U_{2\text{-}1}}{1000} \times \frac{f_{neutral}(f_1 - 1)}{f_{neutral} - 1} + 1 \quad (10)$$

$$y = \quad a \quad \times \quad x \quad + b$$

Equation (10) predicts a linear relationship between $\{f_{neutral}(f_1\text{-}1)/(f_{neutral}\text{-}1)\}$ and observed experimental fractionation. From the slope of the line, it is possible to infer the $\Delta^{238}U_{2\text{-}1}$. Figure 6 shows a plot of linear fitting of Rayleigh isotopic fractionation factors (α) observed in $CaCO_3$ coprecipitation experiments A_1, A_1*, A_3 and C_3 at pH 8.50 versus $\{f_{neutral}(f_1\text{-}1)/(f_{neutral}\text{-}1)\}$. The isotopic fractionation factor in C_1 at pH 8.50 (0.99979 +0.00021/-0.00027) is not included in Fig. 6 because of its large magnitude of fractionation and big uncertainty due to the narrow range of *f* in Rayleigh model fitting. The inferred value of $\Delta^{238}U_{2\text{-}1}$ is 0.32 ± 0.06 ‰, which indicates $\delta^{238}U$ of group 2 is about 0.32 ± 0.06 ‰ heavier than that of group 1. The magnitude of U isotope fractionation between these U species is similar to the range of U isotope fractionation resulting from coordination changes during U adsorption to birnessite, goethite, illite, quartz and aquifer sediments (0.01~0.25 ‰, Brennecka et al., 2011b; Jemision et al., 2014), and U isotope fractionation of $UO_2(CO_3)_3^{4-}$ during ion-exchange chromatography (0.34 ± 0.05 ‰; Aoyama et al., 1989).

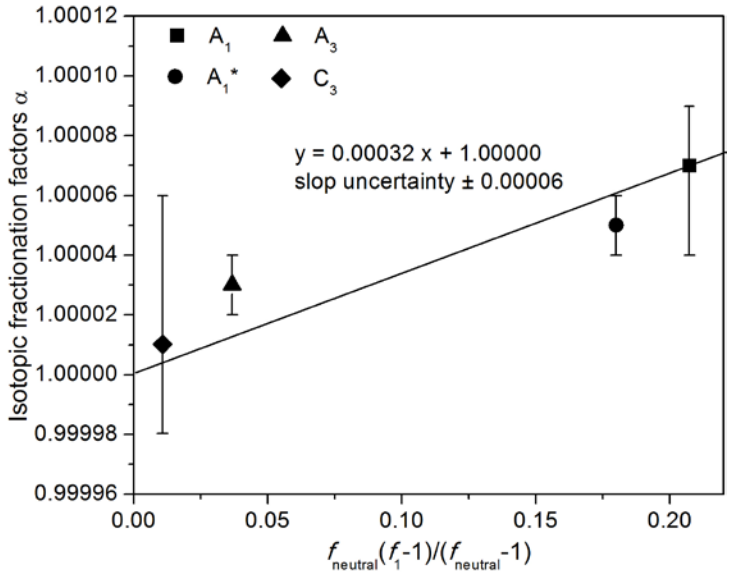

Fig. 6. Linear fitting for Rayleigh isotopic fractionation factors (α) in $CaCO_3$ coprecipitation experiments at pH 8.50 versus $\{f_{neutral}(f_1\text{-}1)/(f_{neutral}\text{-}1)\}$. The filled rectangle, circle, triangle and diamond are Rayleigh isotopic fractionation factors observed in experiments A_1, A_1*, A_3 and C_3.

Using the value of $\Delta^{238}U_{2\text{-}1}$ estimated above, equation (10) can be used to predict the U isotopic fractionation factor (α) as a function of the fraction of neutral U species (Fig. 7), if the relationship between fraction of $Ca_2UO_2(CO_3)_3(aq)$ (f_1) and fraction of U species in Group 1 ($f_{neutral}$) is known.

The relationship between f_1 and $f_{neutral}$ can be derived from U chemical equilibrium. The chemical equilibrium equations of U species in Group 1 are

$$UO_2^{2+} + 3CO_3^{2-} = UO_2(CO_3)_3^{4-}$$

$$K_1 = \frac{\gamma_{UO_2(CO_3)_3^{4-}}\left[UO_2(CO_3)_3^{4-}\right]}{\left(\gamma_{UO_2^{2+}}\left[UO_2^{2+}\right]\right)\left(\gamma_{CO_3^{2-}}\left[CO_3^{2-}\right]\right)^3} \quad (11)$$

$$2Ca^{2+} + UO_2^{2+} + 3CO_3^{2-} = Ca_2UO_2(CO_3)_3(aq)$$

$$K_2 = \frac{\gamma_{Ca_2UO_2(CO_3)_3(aq)}\left[Ca_2UO_2(CO_3)_3(aq)\right]}{\left(\gamma_{UO_2^{2+}}\left[UO_2^{2+}\right]\right)\left(\gamma_{CO_3^{2-}}\left[CO_3^{2-}\right]\right)^3\left(\gamma_{Ca^{2+}}\left[Ca^{2+}\right]\right)^2} \quad (12)$$

$$Ca^{2+} + UO_2^{2+} + 3CO_3^{2-} = CaUO_2(CO_3)_3^{2-}$$

$$K_3 = \frac{\left(\gamma_{CaUO_2(CO_3)_3^{2-}}\left[CaUO_2(CO_3)_3^{2-}\right]\right)}{\left(\gamma_{UO_2^{2+}}\left[UO_2^{2+}\right]\right)\left(\gamma_{CO_3^{2-}}\left[CO_3^{2-}\right]\right)^3\left(\gamma_{Ca^{2+}}\left[Ca^{2+}\right]\right)^2} \quad (13)$$

$$Mg^{2+} + UO_2^{2+} + 3CO_3^{2-} = MgUO_2(CO_3)_3^{2-}$$

$$K_4 = \frac{\left(\gamma_{MgUO_2(CO_3)_3^{2-}}\left[MgUO_2(CO_3)_3^{2-}\right]\right)}{\left(\gamma_{UO_2^{2+}}\left[UO_2^{2+}\right]\right)\left(\gamma_{CO_3^{2-}}\left[CO_3^{2-}\right]\right)^3\left(\gamma_{Mg^{2+}}\left[Mg^{2+}\right]\right)} \quad (14)$$

where K_1, K_2, K_3 and K_4 are equilibrium constants for chemical equilibrium in equations (11) to (14); γ_i is activity coefficient of chemical species (i represents chemical species, for example, UO_2^{2+}); chemical species in square brackets represent the concentration of those species (e.g., $[UO_2^{2+}]$ is the concentration of UO_2^{2+}). The activity coefficient of neutrally-charged U species $Ca_2UO_2(CO_3)_3(aq)$ is assumed to be 1.

Combing equations (11), (12), (13) and (14) the fractions of $UO_2(CO_3)_3^{4-}$, $CaUO_2(CO_3)_3^{2-}$, and $MgUO_2(CO_3)_3^{2-}$ are derived as

$$f_{UO_2(CO_3)_3^{4-}} = \left(\frac{K_1}{K_2} \times \frac{1}{\gamma_{UO_2(CO_3)_3^{4-}}\left(\gamma_{Ca^{2+}}\left[Ca^{2+}\right]\right)^2}\right) \times f_{neutral} \quad (15)$$

$$f_{CaUO_2(CO_3)_3^{2-}} = \left(\frac{K_3}{K_2} \times \frac{1}{\gamma_{CaUO_2(CO_3)_3^{2-}}\left(\gamma_{Ca^{2+}}\left[Ca^{2+}\right]\right)}\right) \times f_{neutral} \quad (16)$$

$$f_{MgUO_2(CO_3)_3^{2-}} = \left(\frac{K_4}{K_2} \times \frac{\left(\gamma_{Mg^{2+}}\left[Mg^{2+}\right]\right)}{\gamma_{MgUO_2(CO_3)_3^{2-}}\left(\gamma_{Ca^{2+}}\left[Ca^{2+}\right]\right)^2}\right) \times f_{neutral} \quad (17)$$

Thus, the relationship between f_1 and $f_{neutral}$ can be described by

$$f_1 = \left(1 + \frac{K_1}{K_2} \times \frac{1}{\gamma_{UO_2(CO_3)_3^{4-}} \left(\gamma_{Ca^{2+}} \left[Ca^{2+}\right]\right)^2}\right) \times f_{neutral} \tag{18}$$

Plugging f_1 in equation (18) into equation (10), the isotopic fractionation factor (α) can be derived as a function of $[Ca^{2+}]$ and $f_{neutral}$ below.

$$\alpha = \frac{\Delta^{238}U_{2\text{-}1}}{1000} \times \frac{\left(f_{neutral}\right)^2}{f_{neutral} - 1} \left(1 + \frac{K_1}{K_2} \times \frac{1}{\gamma_{UO_2(CO_3)_3^{4-}} \left(\gamma_{Ca^{2+}} \left[Ca^{2+}\right]\right)^2}\right) + 1 \tag{19}$$

There are two variables in this function. Thus, it is necessary to get the relationship between $[Ca^{2+}]$ and $f_{neutral}$, which can be described by the restriction that only the four U species are present in aqueous solution. This means that the total fraction of all these U species should be equal to 1. That is the equation

$$\begin{aligned} 1 &= f_{neutral} + f_{UO_2(CO_3)_3^{4-}} + f_{CaUO_2(CO_3)_3^{2-}} + f_{MgUO_2(CO_3)_3^{2-}} \\ &= f_{neutral} + \left(\frac{K_1}{K_2} \times \frac{1}{\gamma_{UO_2(CO_3)_3^{4-}} \left(\gamma_{Ca^{2+}} \left[Ca^{2+}\right]\right)^2}\right) \times f_{neutral} + \left(\frac{K_3}{K_2} \times \frac{1}{\left(\gamma_{Ca^{2+}} \left[Ca^{2+}\right]\right) \gamma_{CaUO_2(CO_3)_3^{2-}}}\right) \times f_{neutral} \\ &\quad + \left(\frac{K_4}{K_2} \times \frac{\left(\gamma_{Mg^{2+}} \left[Mg^{2+}\right]\right)}{\left(\gamma_{Ca^{2+}} \left[Ca^{2+}\right]\right)^2 \gamma_{MgUO_2(CO_3)_3^{2-}}}\right) \times f_{neutral} \\ &= \left(1 + \frac{K_1}{K_2} \times \frac{1}{\gamma_{UO_2(CO_3)_3^{4-}} \left(\gamma_{Ca^{2+}} \left[Ca^{2+}\right]\right)^2} + \frac{K_3}{K_2} \times \frac{1}{\left(\gamma_{Ca^{2+}} \left[Ca^{2+}\right]\right) \gamma_{CaUO_2(CO_3)_3^{2-}}} + \frac{K_4}{K_2} \times \frac{\left(\gamma_{Mg^{2+}} \left[Mg^{2+}\right]\right)}{\left(\gamma_{Ca^{2+}} \left[Ca^{2+}\right]\right)^2 \gamma_{MgUO_2(CO_3)_3^{2-}}}\right) \times f_{neutral} \end{aligned} \tag{20}$$

This equation shows that $f_{neutral}$ only varies as a function of $[Ca^{2+}]$, at constant concentration of Mg^{2+} and ionic strength. Thus, combing equation (19) and (20), the isotopic fractionation factor (α) as a function of the fraction of neutral U species ($f_{neutral}$) can be described.

To predict the relationship between the $f_{neutral}$ and U isotopic fractionation factor (α), the following experimental conditions are used: $[Mg^{2+}]$=50 mM, Ionic strength 0.65 M (A_1 and A_1*); $[Mg^{2+}]$=100 mM, Ionic strength 0.80 M (A_3); $[Mg^{2+}]$=0 mM, Ionic strength 2.0 M (C_3). The activity coefficients of all chemical species are calculated using the software PHREEQC (Parkhurst and Appelo, 2004). With all these conditions and equilibrium constants (K_1, K_2, K_3 and K_4) from Grenthe et al. (1992) and Dong and Brooks (2006), the U isotopic fractionation factor (α) as a function of $f_{neutral}$ at different $[Mg^{2+}]$ are displayed in Fig. 7.

Fig. 7 predicts that isotopic fractionation factor (α) always increases as the fraction of neutral U species increases at different Mg concentrations. This prediction is consistent with our experimental results at pH 8.50. Larger fractionation was observed in experiments A_1 (1.00007 +0.00002/-0.00003) and A_1* (1.00005 ± 0.00001), in which 27% and 24%, respectively, of the dissolved U was present as $Ca_2UO_2(CO_3)_3(aq)$, while smaller U isotope fractionation was seen in experiments A_3 (1.00003 ± 0.00001), which had a fraction of 9% $Ca_2UO_2(CO_3)_3(aq)$. Calcite experiment C_3 showed unresolvable U isotope fractionation with a fraction of 5% $Ca_2UO_2(CO_3)_3(aq)$ in the aqueous solution. All these isotopic fractionation factors lie on their corresponding isotopic fractionation factor lines in Fig. 7.

The agreement between the model and data support the hypothesis that differences in aqueous U speciation prior to incorporation is the likeliest mechanism to explain our results in these experiments.

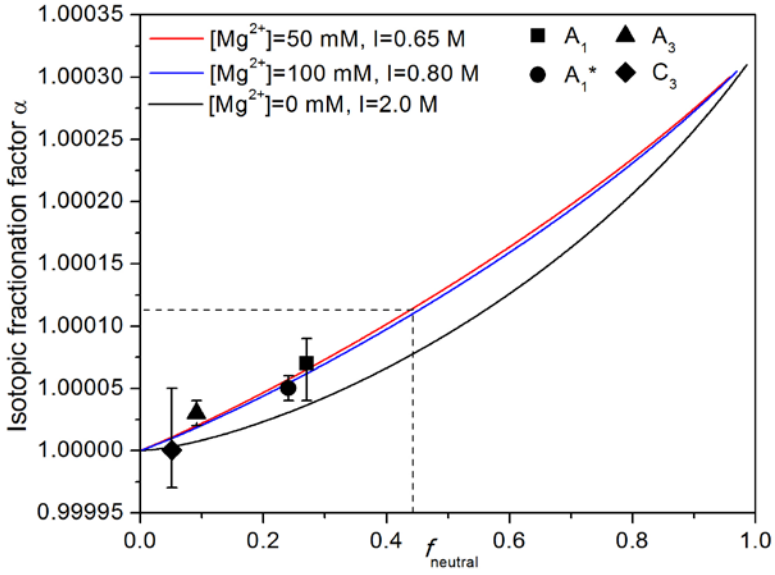

Fig. 7. U isotope fractionation factor (α) between U in instantaneous solid and total dissolved U vs. fraction of neutral U species $Ca_2UO_2(CO_3)_3(aq)$ at different concentrations of Mg^{2+} and ionic strengths. The red, blue and black curves correspond to experimental conditions in A_1 and A_1*, A_3 and C_3. The filled rectangle, circle, triangle and diamond are Rayleigh isotopic fractionation factors observed in experiments A_1, A_1*, A_3, and C_3. The dashed line shows the fraction of neutral U species and the U isotopic composition fractionation predicted for the open ocean.

One limitation of the model discussed above is that it is limited to pH > 8, where only U species in Group 1 and 2 are present. At lower pH (7.50), the presence of U species in Group 3 and 4 are not accounted for by the model. Further experiments would be required to constrain the average U isotopic composition of all charged U species and total dissolved U species ($\Delta^{238}U_{charged\text{-}total}$) in the presence of these new U species. However, even without knowing this value, equation (9) qualitatively predicts that the fractionation in such experiments should be small, because $f_{neutral}$ is small (13% for A_2

and 5% for C_2). This is qualitatively consistent with the unresolvable U isotope fractionation factor observed in aragonite experiment A_2 (1.00001 ± 0.00002).

CHAPTER 5 CONCLUSIONS AND IMPLICATIONS

5.1 Conclusions

The experiments here revealed small fractionation of U isotopes (fractionation factor < 1.00009) during coprecipitation with aragonite. Equilibrium speciation modeling indicates that the magnitude of the fractionation depends on the U speciation. When the fraction of neutral U species $Ca_2UO_2(CO_3)_3(aq)$ in the aqueous solution was larger than 24%, detectable fractionation was observed. When the fraction of this neutral species was < 13%, fractionation was smaller. No resolvable U isotope fractionation was observed in any calcite coprecipitation experiments, all of which had <11% of U present as $Ca_2UO_2(CO_3)_3(aq)$. When fractionation was observed, Rayleigh-type behavior was seen, with heavier U isotopes preferentially incorporated into aragonite at pH 8.5.

Equilibrium isotope fractionation between different aqueous U species prior to incorporation is proposed as the likeliest mechanism to explain these results. Specifically, we hypothesize a fractionation between the uncharged species $Ca_2UO_2(CO_3)_3(aq)$ and most of the dissolved charged species, favoring light U isotopes in $Ca_2UO_2(CO_3)_3(aq)$. Fractionation arises because charged U species are more readily incorporated into the minerals during precipitation. The relative abundance of this uncharged species was greatest in our aragonite experiments, potentially explaining why fractionation was seen in these experiments. Further work is needed to test this hypothesis such as by quantum chemical modeling of U isotope fractionation between $Ca_2UO_2(CO_3)_3$ and other U species.

5.2 Implications

The experimental results here suggest that U speciation in seawater may be the key factor controlling U isotope fractionation during incorporation into abiotic carbonates. Due to constraints in the experimental design, the aqueous speciation of U in the experiments reported here does not exactly match U speciation predicted for modern open ocean seawater. U speciation modeling using the software PHREEQC (Parkhurst and Appelo, 2004) indicates four U species are expected to be present in modern seawater: $CaUO_2(CO_3)_3^{2-}$ (36%), $MgUO_2(CO_3)_3^{2-}$ (14%), $Ca_2UO_2(CO_3)_3$(aq) (45%), and $UO_2(CO_3)_3^{4-}$ (5%) at pH 8.22. Notably, seawater is predicted to have more neutrally-charged $Ca_2UO_2(CO_3)_3$(aq) than was present in our experiments. By using the relationships inferred from our study (e.g., Fig. 7), we can extrapolate to seawater conditions. This extrapolation suggest that abiotic $CaCO_3$ precipitation in modern seawater may result in an isotope fractionation factor of 1.00009-1.00013, and therefore that the U isotopic composition in instantaneous $CaCO_3$ may be 0.11 ± 0.02‰ heavier than that of total dissolved U in seawater.

To date, almost all measurements of primary carbonate precipitates show U isotopic compositions similar to seawater (Weyer et al., 2008; Romaniello et al., 2013). However, almost all of these samples are biological precipitates (e.g., coral and calcifying green and red algae). If our prediction of the U isotope fractionation during U incorporation into abiotic calcium carbonate in seawater is right, then biological processes may lead to smaller U isotope fractionation during U uptake by biotic $CaCO_3$ than during abiotic precipitation. Such processes include those that cause changes in $[Mg^{2+}]$, $[Ca^{2+}]$, $[CO_3^{2-}]$, or pH at the calcification sites. For example, in situ pH

microelectrode and B isotopes analyses have demonstrated that some biological carbonates elevate pH as much as ~1 unit above the seawater pH (8.2) in the calcification sites, facilitating $CaCO_3$ precipitation with high oversaturation (Zeebe et al., 2003; Trotter et al., 2011; Rollion-Bard and Erez, 2009; Nooijer et al., 2009; Al-Horani et al, 2003). The elevation of pH by ~1 unit can lead to significant increase in $[CO_3^{2-}]$ (~90%, Nooijer et al., 2009). Additionally, $[Ca^{2+}]$ and $[Mg^{2+}]$ in the calcification fluids are lower than in seawater (Weiner and Dove, 2003). The decreased $[Ca^{2+}]$ and $[Mg^{2+}]$, and elevated $[CO_3^{2-}]$ in the calcification sites should reduce the fraction of U present as the neutral U species $Ca_2UO_2(CO_3)_3(aq)$. This change may reduce U isotopic fractionation during U coprecipitation with $CaCO_3$.

The non-resolvable U isotope fractionation between seawater and modern biogenic carbonates suggests that U isotopes in biotic marine carbonates might be a reliable paleoredox proxy. However, to use U isotopes in abiotic carbonates as a paleoredox proxy might require corrections, which depend on the U speciation in seawater.

REFERENCES

Algeo T. J. and Maynard J. B. (2004) Trace-element behavior and redox facies in core shales of Upper Pennsylvanian Kansas-type Cyclothems. *Chem. Geol.* **206**, 289-318.

Algeo T. J. and Rowe H. (2011) Paleoceanographic applications of trace-metal concentration data. *Chem. Geol.* **324-325**, 6-18.

Al-Horani F. A., Al-Moghrabi S. M. and de Beer D. (2003) The mechanism of calcification and its relation to photosynthesis and respiration in the scleractinian coral *galaxea fascicularis*. *Mar Biol.* **142**, 419-426.

Alibo D. S. and Nozaki Y. (1999) Rare earth elements in seawater: Particle association, shale-normalization, and Ce oxidation. *Geochim. Cosmochim. Acta* **63**, 363-372.

Anbar A. D. and Knoll A. H. (2002) Proterozoic ocean chemistry and evolution: A bioinorganic bridge? *Science* **297**, 1136-1142.

Andersen M. B., Romaniello S., Vance D., Little S. H., Herdman R. and Lyons T. W. (2014) A modern framework for the interpretation of $^{238}U/^{235}U$ in studies of ancient ocean redox. *Earth Planet. Sci. Lett.* **400**, 184-194.

Anderson R. F., Fleisher M. Q. and Lehuray A. P. (1989) Concentration, oxidation state, and particulate flux of uranium in the Black Sea. *Geochim. Cosmochim. Acta* **53**, 2215-2224.

Aoyama T., Aida M., Fujii Y. and Okamoto M. (1989) Uranium isotope effects in uranyl carbonate complex system. *J. Phys. Chem*. **93**, 2666-2668.

Asael D., Tissot F. L. H., Reinhard C. T., Rouxel O., Dauphas N., Lyons T. W., Ponzevera E., Liorzou C. and Cheron S. (2013) Coupled molybdenum, iron and uranium stable isotopes as oceanic paleoredox proxies during the Paleoproterozoic Shunga Event. *Chem. Geol.* **362**, 193-210.

Bogatko S., Claeys P., Proft F. D. and Geerlings P. (2013) Li^+ speciation and the use of $^7Li/^6Li$ isotope ratios for ancient climate monitoring. *Chem. Geol.* **357**, 1-7.

Barling, J., Anbar, A. D. (2004) Molybdenum isotope fractionation during adsorption by manganese oxides. *Earth Planet. Sci. Lett.* **217**, 315-329.

Basu A. (2013) Isotopic fractionation of chromium and uranium during abiotic and microbial Cr(VI) reduction and microbial U(VI) reduction. Ph.D. thesis, UIUC.

Bernhard G., Geipel G., Reich T., Brendler V., Amayri, S. and Nitsche H. (2001) Uranyl(VI) carbonate complex formation: Validation of the $Ca_2UO_2(CO_3)_3(aq)$ Species. *Radiochim. Acta*. **89**, 511−518.

Berner R. A., VandenBrooks J. M. and Ward P. D. (2007) Oxygen and evolution. *Science* **316**, 557-558.

Bigeleisen J. (1996) Nuclear size and shape effects in chemical reactions. isotope chemistry of the heavy elements. *J. Am. Chem. Soc.***118**, 4676-3680.

Bopp C. J., Lundstron C. C., Johnson T. M. and Glessner J. J. G. (2009) Variations in $^{238}U/^{235}U$ in the uranium ore deposits: Isotopic signatures of the U reduction process? *Geology* **37**, 611-614.

Bopp C. J., Lundstrom C. C., Johnson T. M., Sanfor R. A., Long P. E. and Wiliams K. H. (2010) Uranium $^{238}U/^{235}U$ isotope ratio as indicators of reduction: Result from an in situ biostimulation experiment at Rile, Colorado, U. S. A. *Environ. Sci. Technol.***44**, 5927-5933.

Brennecka G. A., Borg L. E., Hutcheon I. D., Sharp M. A. and Anbar A. D. (2010) Natural variations in uranium isotope ratios of uranium ore concentrate: Understanding the $^{238}U/^{235}U$ fractionation mechanism. *Earth. Planet. Sci. Lett.* **291**, 228-233.

Brennecka G. A., Herrmannn A. D., Algeo T. J. and Anbar, A.D. (2011) Rapid expansion of oceanic anoxia immediately before the End-Permian Mass Extinction. *Proc. Natl. Acad. Sci.* **108**, 17631-17634.

Brennecka G. A., Wasylenki L.E., Bargar J.R., Weyer S. and Anbar, A.D. (2011) Uranium isotope fractionation during adsorption to Mn-oxyhydroxides. *Environ. Sci. Technol.* **45**, 1370-1375.

Bryan A. L., Dong S., Wilkes E. B. and Wasylenki L. E. (2015) Zinc isotope fractionation during adsorption onto Mn oxyhydroxide at low and high ionic strength. *Geochim. Cosmochim. Acta* **157**, 182-197.

Canfield D. E., Poulton S. W. and Narbonne G. W. (2007) Late-Neoproterozoic deep-ocean oxygenation and the rise of animal life. *Science* **315**, 92-95.

Chung G. S. and Swart P. K. (1990) The concentration of uranium in freshwater vadose and phreatic cements in a Holocene ooid cays: A method of identifying ancient water tables. *J. Sediment. Petrol.* **60**, 735-746.

Colla C. A., Wimpenny J., Yin Q., Rustad J. R. and Casey W. H. (2013) Calcium-isotope fractionation between solution and solids with six, seven, or eight oxygens bound to Ca(II). *Geochim. Cosmochim. Acta* **121**, 363-373.

Dahl T. W., Boyle R. A., Canfield D. E., Connelly J. N., Gill B. C., Lenton T. M. and Bizzarro M. (2014) Uranium isotopes distinguish two geochemically distinct stages during the later Cambrian SPICE Event. *Earth Planet. Sci. Lett.* **401**, 313-326.

Docrat T., Mosselmans J., Charnock J., Whiteley M., Collision D., Livens F., Jones C. and Edmiston M. (1999) X-Ray absorption spectroscopy of tricarbonatodioxouranate(V), $[UO_2(CO_3)_3]^{5-}$, in aqueous solution. *Inorg. Chem.* **38**, 1879-1882.

Dong W. and Brooks S. C. (2006) Determination of the formation constants of ternary complexes of uranyl and carbonate with alkaline earth metals (Mg^{2+}, Ca^{2+}, Sr^{2+}, and Ba^{2+}) using anion exchange method. *Environ. Sci. Technol.* **40**, 4689-4695.

Dong W., Ball W. P., Liu C., Wang Z., Stone A. T., Bai J. and Zachara J. M. (2005) Influence of calcite and dissolved calcium on uranium(VI) sorption to a Hanford subsurface sediment. *Environ. Sci. Technol.* **39**, 7949-7955.

Dunk R. M., Mills R. A. and Jenkins W. J. (2002) A reevaluation of the oceanic uranium budget for the Holocence. *Chem. Geol.* **190**, 45-67.

Elzinga E. J., Tait C. D., Reeder R. J., Rector K. D., Donohoe R. J. and Morris D. E. (2004) Spectroscopic investigation of U(VI) sorption at the calcite-water interface. *Geochim. Cosmochim. Acta* **68**, 2437-2448.

Fox P. M., Davis J. A. and Zachara J. M. (2006) The effect of calcium on aqueous uranium(VI) speciation and adsorption to ferrihydrite and quartz. *Geochim. Cosmochim. Acta* **70**, 1379-1387.

Fujii T., Moynier F., Abe M., Nemoto K. and Albarede F. (2013) Copper isotope fractionation between aqueous compounds relevant to low temperature geochemistry and biology. *Geochim. Cosmochim. Acta* **110**, 29-44.

Gabitov R. I., Gaetani G. A., Watson E. B., Cohen A. L. and Ehrlich H. L. (2008) Experimental determination of growth rate effect on U^{6+} and Mg^{2+} partitioning between aragonite and fluid at elevated U^{6+} concentration. *Geochim. Cosmochim. Acta* **72**, 4058-4068.

German, C. R. and Elderfield, H. (1990) Application of the Ce anomaly as a paleoredox indicator: the ground rules. *Paleoceanography* **5**, 823-833.

Gill B. C., Lyons T. W. and Frank T. D. (2008) Behavior of carbonate-associated sulfate during meteoric diagenesis and implications for the sulfur isotope paloeproxy. *Geochim. Cosmochim. Acta* **72**, 4699-4711.

Grenthe I., Fuger J., Konings R. J. M., Lemire R. J., Muller A. B., Gregu C. N. T. and Wanner H. (1992) *Chemical Thermodynamics 1: Chemical Thermodynamics of Uranium*. North-Holland Elsevier Science: New York.

Guillaumont R., Fanghanel T., Fuger J., Grenthe I., Neck V., Palmer D. and Rand M. H. (2003) *Update on the Chemical Thermodynamics of Uranium, Neptonium, Plutonium, Americium and Technetium.* Elsevier: Amsterdam.

Hardisty D. S., Lu Z., Planavsky N. J., Bekker A., Philippot P., Zhou X. and Lyons T. W. (2014). An iodine record of Paleoproterozoic surface ocean oxygenation. *Geology* **42,** 619-622.

Herrmannn A. D., Kendall B., Algeo T. J., Gordon G. W., Wasylenki L. E. and Anbar A. D. (2012) Anomalous molybdenum isotope trends in Upper Pennsylvanian euxinic facies: Significance for use of δ^{98}Mo as a global marine redox proxy. *Chem. Geol.* **324**, 87-98.

Howard A. G. and Statham P. J. (1993) Inorganic *Trace Analysis: Philosophy and Practice*. *Wiley*, Chichester.

Huang F., Wu Z., Huang S. and Wu F. (2014) First-principles calculations of equilibrium silicon isotope fractionation among mantle minerals. *Geochim. Cosmochim. Acta* **140**, 509-520.

Jemison N., Johnson T. M., Shiel A. E. and Lundstrom C. C. (2014) Uranium isotopic fractionation induced by U(VI) adsorption onto common aquifer minerals. *AGU Fall Meeting*, San Francisco, CA. #22730 (abstr.).

Juillot F., Marechal C., Ponthieu M., Cacaly S., Morin G., Benedetti M. and Guyot F. (2008) Zn isotopic fractionation caused by sorption on goethite and 2-lines ferrihydrite. *Geochim. Cosmochim. Acta* **72**, 4886-4900.

Kakuwa, Y. and Matsumoto, R. (2006) Cerium negative anomaly just before the Permian and Triassic Boundary Event - the upward expansion of anoxia in the water column. *Palaeogeogr. Palaeoclimatol. Palaeoecol.* **229**, 335-344.

Kelly S. D., Newville M. G., Cheng, L., Kemner K. M., Sutton S. R., Fenter P., Sturchio N. C. and Spotl C. (2003) Uranyl incorporation into natural calcite. *Environ. Sci. Technol.* **37**, 1284-1287.

Kelly S. D., Rasbury E. T., Chattopadhyay S., Kropf A. J. and Kemner K. M. (2006) Evidence of a stable uranyl site in ancient organic-rich calcite. *Environ. Sci. Technol.***40**, 2262-2268.

Kendall B., Brennecka G. A., Weyer S. and Anbar. A. D. (2013) Uranium isotope fractionation suggests oxidative uranium mobilization at 2.50 Ga. *Chem. Geol.* **362**, 105-114.

Kerisit S. and Liu C. (2010) Molecular simulation of the diffusion of uranyl carbonate species in aqueous solution. *Geochim. Cosmochim. Acta* **74**, 4937-4952.

Klinkhammer G. P. and Palmer M. R. (1991) Uranium in the oceans: Where it goes and why. *Geochim. Cosmochim. Acta* **55**, 1799-1806.

Kowalski P. M. and Jahn S. (2011) Prediction of equilibrium Li isotope fractionation between minerals and aqueous solutions at high *P* and *T*: An efficient *ab initio* approach. *Geochim. Cosmochim. Acta* **75**, 6112-6123.

Langmuir D. (1978) Uranium solution-mineral equilibria at low temperatures with applications to sedimentary ore deposits. *Geochim. Cosmochim. Acta* **42**, 547-569.

Lazar B., Enmar R., Schossberger M., Bar-Matthews M., Halicz L. and Sten M. (2004) Diagenetic effects on the distribution of uranium in live and Holocene corals from the gulf of Aqaba. *Geochim. Cosmochim. Acta* **22**, 4583-4593.

Li Y., Zhao L., Chen Z., Chen J. and Chen Y. (2013) Rare earth elements of the Permian-Triassic Conodonts from shelf basin to shallow platform: Implications for oceanic redox conditions immediately after the End-Permian Mass Extinction. *AGU Fall Meeting*, San Franciso, CA. #V33E-2811.

Little S. H., Sherman D. M., Vance D. and Hein J. R. (2014) Molecular controls on Cu and Zn isotopic fractionation in Fe-Mn crusts. *Earth Planet. Sci. Lett.* **396**, 213-222.

Lu Z., Jenkyns H. C. and Rickaby R. E. M. (2010) Iodine to calcium ratios in marine carbonate as a paleo-redox proxy during oceanic anoxic events. *Geology* **38**, 1107-1110.

Ludwig, K. R. (2012) Isoplot, A geochronological toolkit for microsoft excel. Berkeley Geochronology Center, Special Publication No. 5, p.75.

Lyons T. W., Anbar A. B., Severmann S., Scott C. and Gill B. C. (2009) Tracking Euxinia in the Ancient Ocean: A multiproxy perspective and Proterozoic case study. *Annu. Rev. Earth. Planet. Sci.* **37**, 507-534.

Mariotti A., Germon J. C. Hubert P., Kaiser P., Letolle R., Tardieux A. and Tardieux P. (1981) Experimental determination of nitrogen kinetic isotope fractionation: Some principles; illustration for the denitrification and nitrification process, *Plant Soil* **62**, 413-430.

Martin G. D., Wilkinson B. H. and Lohmann K. C. (1986) The role of skeletal porosity in aragonite neomorphism-*strombus* and *montastrea* from Pleistocence Key Largo Limestone, Florida. *J. Sediment. Petrol.* **56**, 194-203.

McManus J., Berelson W. M., Kilnkhamer G. P., Hammond D. E. and Holm C. (2005) Authigenic uranium: Relationship to oxygen penetration depth and organic carbon rain. *Geochim. Cosmochim. Acta* **69**, 95-108.

Montoya-Pino C., Weyer S., Anbar A. D., Pross J., Oschmann W., Schootbrugge B. V. and Arz H. W. (2010) Global enhancement of ocean anoxia during oceanic anoxic event 2: A quantitative approach using U isotopes. *Geology* **38**, 315-318.

Morford J. L. and Emerson. (1999) The geochemistry of redox sensitive srace metals in sediments. *Geochim. Cosmochim. Acta* **63**, 1735-1750.

Morse J. W. and Mackenzie F. T. (1990) *Geochemistry of Sedimentary Carbonates*. Elsevier, New York.

Morse J. W., Wang Q. and Tiso M. Y. (1997) Influences of temperature and Mg:Ca Ratio on $CaCO_3$ precipitates from seawater. *Geology* **25**, 85-87.

Nielsen S. G., Wasylenki L. E., Rehkamper M., Peacock C. L., Xue Z. and Moon E. M. (2013) Towards an understanding of thallium isotope fractionation during adsorption to manganese oxides. *Geochim. Cosmochim. Acta* **117**, 252-265.

Nooijer L. J. D., Toyofuku T. and Kitazato H. (2009) Foraminifera promote calcification by elevating their intracellular pH. *Proc. Natl. Acad. Sci.* **106**, 15374-15378.

Ortega R., Maire R., Deves G. and Quinif Y. (2005) High-resolution mapping of uranium and other trace elements in recrystallized aragonite–calcite speleothems from caves in the Pyrenees (France): Implication for U-series dating. *Earth Planet. Sci. Lett.* **237**, 911-923.

Pufahl P. K. and Hiatt E. E. (2012) Oxygenation of the Earth's atmosphere-ocean System: A review of physical and chemical sedimentologic responses. *Mar. Petrol. Geol.* **32**, 1-20.

Parkhurst D. L. and Appelo C. A. (2004) *User's Guide to PHREEQC (Version 2) – A Computer Program for Speciation, Batch-Reaction, One-Dimension Transport, and Inverse Geochemical Calculations*. U. S. Geological Survey: Reston, VA.

Reeder R. J., Nugent M., Lamble G. M., Tait C. D. and Morris D. E. (2000) Uranyl incorporation into calcite and aragonite: XAFS and luminescence studies. *Environ. Sci. Technol.* **34**, 638-644.

Reeder R. J., Nugent M., Tait C. D., Morris D. E., Heald S. M., Beck K. M., Hess W. P. and Lanzirotti A. (2001) Coprecipitation of uranium(VI) with calcite: XAFS, micro-XAS, and luminescence characterization. *Geochim. Cosmochim. Acta* **65**, 3491-3503.

Rollion-Bard C. and Erez J. (2010) Intra-shell boron isotope ratios in the symbiont-bearing benthic foraminiferan *amphistegina lobifera*: Implications for $\delta^{11}B$ vital effects and paleo-pH reconstructions. *Geochim. Cosmochim. Acta* **74**, 1530-1536.

Romaniello S. J., Herrmann A. D. and Anbar A. D. (2013) Uranium concentrations and $^{238}U/^{235}U$ isotope ratios in modern carbonates from the Bahamas: Assessing a novel paleoredox proxy. *Chem. Geol.* **362**, 305-316.

Ronov A. B. (1964) Common tendencies in the chemical evolution of the Earth's crust, ocean and atmosphere. *Geochem. Intl*. **1**, 713-737.

Rudge J. F., Reynolds B. C. and Bourdon B. (2009) The double spike toolbox. *Chem. Geol.* **265**, 420-431.

Schauble E. A. (2004) Applying stable isotope fractionation theory to new systems, geochemistry of non-traditional stable isotopes. *Rev. Mineral. Geochem.* **55**, 65-111.

Schauble E. A. (2007) Role of nuclear volume in driving equilibrium stable isotope fractionation of mercury, thallium, and other very heavy elements. *Geochim. Cosmochim. Acta* **71**, 2170-2189.

Scott C., Lyons T. W., Bekker A., Shen Y., Poulton S. W., Chu X. and Anbar A. D. (2008) Tracing the stepwise oxygenation of the Proterozoic ocean. *Nature* **452**, 456-461.

Scott C. T., Bekker A., Reinhard C. T., Schnetger B., Krapez B., Rumble III D. and Lyons T. W. (2011) Late archean euxinic conditions before the rise of atmospheric oxygen. *Geology* **39**, 119-122.

Shields G. and Veizer J. (2002) Precambrian marine carbonate isotope database: Version 1.1. *Geochem. Geophys. Geosyst.* **3**, 1-12.

Shiel A. E., Laubach P. G., Johnson T. M., Lundstrom C. C., Long P. E. and Williams K. H. (2013) No measurable changes in $^{238}U/^{235}U$ due to desorption-adsorption of U(VI) from groundwater at the Rifle, Colorado, integrated field research challenge site. *Environ. Sci. Technol.* **47**, 2535-2541.

Stirling C. H., Andersen M. B., Potter E. K. and Halliday A. N. (2007) Low-temperature isotopic fractionation of Uranium. *Earth. Planet. Sci. Lett.* **264**, 208-225.

Szabo Z., Moll H. and Grenthe I. (2000) Structure and dynamics in the complex ion $(UO_2)_2(CO_3)(OH)_3^-$. *J. Chem. Soc., Dalton Trans.* **18**, 3158-3161.

Tribovillard N., Algeo, T. J., Lyons T. and Riboulleau A. (2006) Trace metals as paleoredox and paleoproductivity proxies: An update. *Chem. Geol.* **232**, 12-32.

Trotter J., Montagna P., McCulloch M., Silenzi S., Reynaud S., Mortimer G., Martin S., Ferrier-Pages C., Gattuso J. P. and Rodolfo-Metalpa R. (2011) Quantifying the pH 'vital effect' in the temperature zooxanthellate coral *cladocora caespitosa*: Validation of the boron seawater pH proxy. *Earth. Planet. Sci. Lett.* **303**, 163-173.

Tunusoglu O. (2007) Kinetic, morphological, and compositional characterization of the uptake of aqueous Ba^{2+}, Mn^{2+}, and Cd^{2+} ions by calcite and aragonite over a wide range of concentration. Master Thesis, Izmir Institute of Technology.

Vallet V., Wahlgren U. and Grenthe I. (2012) Probing the nature of chemical bonding in uranyl(VI) complexes with quantum chemical methods. *J. Phys. Chem.* **116**, 12373-12380.

Verbruggen A., Alonso-Munoz A., Eykens R., Kehoe F., Kuhen H., Richter S. and Arbegbe Y. (2008) Preparation and certification of IRMM-3636, IRMM-3636a and IRMM-3636b. OPOCE, *24pp*.

Wang Z., Zachara J. M., Mckinley J. P. and Smith Steven. (2005) Cryogenic laser induced U(VI) fluorescence studies of a U(IV) substituted natural calcite: Implications to U(VI) speciation in contaminated Hanford sediments. *Environ. Sci. Technol.* **39**, 2651-2659.

Wasylenki L. E., Weeks C. L., Bargar J. R., Spiro T. G., Hein J. R. and Anbar A. D. (2011) The molecular mechanism of Mo isotope fractionation during adsorption to birnessite. *Geochim. Cosmochim. Acta* **75**, 5109-5031.

Weiner S. and Dove P. M. (2003) An overview of biomineralization processes and the problem of the vital effect. *Rem. Mineral. Geochem.* **54**, 1-29.

Weyer S., Anbar A. D., Gerdes A., Gordon G. W., Algeo T. J. and Bolye E. A. (2008) Natural fractionation of $^{238}U/^{235}U$. *Geochim. Cosmochim. Acta* **72**, 345-359.

Wignall P. B. and Twitchett R. J. (1996) Oceanic anoxia and the End Permian Mass Extinction. *Science* **272**, 1155-1158.

Wilkinson B. H. and Walker J. C. G. (1989) Phanerozoic cycling of sedimentary carbonate. *Amer. J. Sci.* **289**, 525-548.

Wunder S. J. (1974) Diagenetic features and inferred diagenetic processes in partially altered corals from the Key Largo Limestone (Pleistocence) South Florida. Master Thesis, University of Illinois-Urbana.

York, D. (1966) Least-squares fitting of a straight line. *Can. Jour. Phys.* **44**, 1079-1086.

Zeebe R. (2005) Stable boron isotope fractionation between dissolved $B(OH)_3$ and $B(OH)_4^-$. *Geochim. Cosmochim. Acta* **69**, 2753-2766.

Zeebe R., Wolf-Gladrow D. A., Bijma J. and Honisch B. (2003). Vital effects in foraminifera do not compromise the use of $\delta^{11}B$ as a paleo-pH indicator: Evidence from modeling. *Paleoceanography* **18**, 21-29.

Zheng Z., Tokunaga T. K. and Wan J. (2003) Influence of calcium carbonate on U(VI) sorption to soils. *Environ. Sci. Technol.* **37**, 5603-5608.

Zhong S. and Mucci. (1996) Calcite precipitation in seawater using a constant addition technique: A new overall reaction kinetic expression. *Geochim. Cosmochim. Acta* **57**, 1409-1417.

Zhou X., Jenkyns H. C., Owens J. D., Junium C. K., Zheng X., Sageman B. B., Hardisty D. S., Lyons T. W., Ridgwell A. and Lu Z. (2015) Upper ocean oxygenation dynamics from I/Ca ratios during the Cenomanian-Turonian OAE 2. *Oceanography* **30**, 510-526.

APPENDIX A

EQUATIONS DERIVATIONS

Derivations of equations (8) and (10) from equations (5), (6), and (7).

$$(\alpha\text{-}1) \times 1000 \approx \delta^{238}U_{instantaneous} - \delta^{238}U_{total} = \delta^{238}U_{charged} - \delta^{238}U_{total} \quad (5)$$

$$f_{neutral} \times \delta^{238}U_{neutral} + (1 - f_{neutral}) \times \delta^{238}U_{charged} = \delta^{238}U_{total} \quad (6)$$

$$f_1 \times \delta^{238}U_1 + (1 - f_1) \times (\delta^{238}U_1 + \Delta^{238}U_{2\text{-}1}) = \delta^{238}U_{total} \quad (7)$$

Because the neutral U species - $Ca_2UO_2(CO_3)_3(aq)$ - is one member of the U species in Group 1, $\delta^{238}U_{neutral}$ is equal to $\delta^{238}U_1$. Using this information, equation (7) can be rewritten as

$$\delta^{238}U_{neutral} + (1 - f_1) \times \Delta^{238}U_{2\text{-}1} = \delta^{238}U_{total} \quad (7a)$$

If we define the difference of isotopic composition between neutral U species and total dissolved U species as $\Delta^{238}U_{neutral\text{-}total} (= \delta^{238}U_{neutral} - \delta^{238}U_{total})$, equation 7(a) will be

$$\Delta^{238}U_{neutral\text{-}total} = (f_1 - 1) \times \Delta^{238}U_{2\text{-}1} \quad (8)$$

From equation (6), $\delta^{238}U_{charged}$ can be derived as:

$$\delta^{238}U_{charged} = \frac{\delta^{238}U_0 - f_{neutral} \times \delta^{238}U_{neutral}}{1 - f_{neutral}} \quad (6a)$$

Plug in $\delta^{238}U_{charged}$ into equation (5), we can get

$$\begin{aligned}
(\alpha\text{-}1) \times 1000 &= \delta^{238}U_{charged} - \delta^{238}U_0 \\
&= \frac{\delta^{238}U_0 - f_{neutral} \times \delta^{238}U_{neutral}}{1 - f_{neutral}} - \delta^{238}U_0 \\
&= \frac{\delta^{238}U_0 - f_{neutral} \times \delta^{238}U_{neutral} - (1 - f_{neutral}) \times \delta^{238}U_0}{1 - f_{neutral}} \quad (5b) \\
&= \frac{(\delta^{238}U_0 - \delta^{238}U_{neutral}) f_{neutral}}{1 - f_{neutral}} \\
&= \frac{f_{neutral}}{f_{neutral} - 1} \Delta^{238}U_{neutral\text{-}total}
\end{aligned}$$

Thus, the isotopic fractionation factor (α) can be derived as

$$\alpha = \frac{\Delta^{238}U_{\text{neutral-total}}}{1000} \times \frac{f_{\text{neutral}}}{f_{\text{neutral}}\text{-}1} + 1 \tag{5c}$$

Substitute equation (8) into equation (5c), we can get the equation (10) below

$$\begin{aligned} \alpha &= \frac{\Delta^{238}U_{\text{neutral-total}}}{1000} \times \frac{f_{\text{neutral}}}{f_{\text{neutral}}\text{-}1} + 1 \\ &= \frac{(f_1\text{-}1) \times \Delta^{238}U_{2\text{-}1}}{1000} \times \frac{f_{\text{neutral}}}{f_{\text{neutral}}\text{-}1} + 1 \\ &= \frac{\Delta^{238}U_{2\text{-}1}}{1000} \times \frac{(f_1\text{-}1)f_{\text{neutral}}}{f_{\text{neutral}}\text{-}1} + 1 \end{aligned} \tag{10}$$

Derivation of equations (18), (19) and (20)

$$UO_2^{2+} + 3CO_3^{2-} = UO_2(CO_3)_3^{4-}$$

$$K_1 = \frac{\gamma_{UO_2(CO_3)_3^{4-}}\left[UO_2(CO_3)_3^{4-}\right]}{\left(\gamma_{UO_2^{2+}}\left[UO_2^{2+}\right]\right)\left(\gamma_{CO_3^{2-}}\left[CO_3^{2-}\right]\right)^3} \tag{11}$$

$$2Ca^{2+} + UO_2^{2+} + 3CO_3^{2-} = Ca_2UO_2(CO_3)_3(aq)$$

$$K_2 = \frac{\gamma_{Ca_2UO_2(CO_3)_3(aq)}\left[Ca_2UO_2(CO_3)_3(aq)\right]}{\left(\gamma_{UO_2^{2+}}\left[UO_2^{2+}\right]\right)\left(\gamma_{CO_3^{2-}}\left[CO_3^{2-}\right]\right)^3\left(\gamma_{Ca^{2+}}\left[Ca^{2+}\right]\right)^2} \tag{12}$$

Equation (11) divided be equation (12), we can get

$$\frac{K_1}{K_2} = \frac{\left(\gamma_{O_2(CO_3)_3^{4-}}\left[UO_2(CO_3)_3^{4-}\right]\right)\left(\gamma_{Ca^{2+}}\left[Ca^{2+}\right]\right)^2}{\left(\gamma_{Ca_2UO_2(CO_3)_3(aq)}\left[Ca_2UO_2(CO_3)_3(aq)\right]\right)} \tag{11a}$$

The activity coefficient of neutrally-charged U species - $Ca_2UO_2(CO_3)_3(aq)$ - is assumed to be 1. From equation (11a), the concentration ratio of $UO_2(CO_3)_3^{4-}$ to $Ca_2UO_2(CO_3)_3(aq)$ is

$$\frac{\left[UO_2(CO_3)_3^{4-}\right]}{\left[Ca_2UO_2(CO_3)_3(aq)\right]} = \frac{K_1}{K_2} \times \frac{1}{\left(\gamma_{Ca^{2+}}\left[Ca^{2+}\right]\right)^2 \gamma_{UO_2(CO_3)_3^{4-}}} \tag{11b}$$

Thus, the total fraction of U species in Group 1 ($UO_2(CO_3)_3^{4-}$ and $Ca_2UO_2(CO_3)_3(aq)$) is

$$\begin{aligned} f_1 &= f_{neutral} + \frac{\left[UO_2(CO_3)_3^{4-}\right]}{\left[Ca_2UO_2(CO_3)_3(aq)\right]} \times f_{neutral} \\ &= f_{neutral} + \left(\frac{K_1}{K_2} \times \frac{1}{\gamma_{UO_2(CO_3)_3^{4-}} \left(\gamma_{Ca^{2+}}\left[Ca^{2+}\right]\right)^2} \right) \times f_{neutral} \\ &= \left(1 + \frac{K_1}{K_2} \times \frac{1}{\gamma_{UO_2(CO_3)_3^{4-}} \left(\gamma_{Ca^{2+}}\left[Ca^{2+}\right]\right)^2} \right) \times f_{neutral} \end{aligned} \tag{18}$$

Substitute f_1 in equation (18) into equation (10), the U isotopic fractionation factor (α) can be written as a function of the fraction of neutral U species and $[Ca^{2+}]$ as follows:

$$\begin{aligned} \alpha &= \frac{\Delta^{238}U_{2\text{-}1}}{1000} \times \frac{(f_1\text{-}1) f_{neutral}}{f_{neutral}\text{-}1} + 1 \\ &= \frac{\Delta^{238}U_{2\text{-}1}}{1000} \times \frac{f_{neutral}}{f_{neutral}\text{-}1} \times \left(1 + \frac{K_1}{K_2} \times \frac{1}{\gamma_{UO_2(CO_3)_3^{4-}} \left(\gamma_{Ca^{2+}}\left[Ca^{2+}\right]\right)^2} \right) \times f_{neutral} + 1 \\ &= \frac{\Delta^{238}U_{2\text{-}1}}{1000} \times \frac{\left(f_{neutral}\right)^2}{f_{neutral}\text{-}1} \times \left(1 + \frac{K_1}{K_2} \times \frac{1}{\gamma_{UO_2(CO_3)_3^{4-}} \left(\gamma_{Ca^{2+}}\left[Ca^{2+}\right]\right)^2} \right) + 1 \end{aligned} \tag{19}$$

Similar to the derivation of the concentration ratio of $UO_2(CO_3)_3^{4-}$ to $Ca_2UO_2(CO_3)_3(aq)$, the ratio $[CaUO_2(CO_3)_3^{2-}]$ to $[Ca_2UO_2(CO_3)_3(aq)]$ can be get from equations (11) and (13).

$$\frac{\left[CaUO_2(CO_3)_3^{2-}\right]}{\left[Ca_2UO_2(CO_3)_3(aq)\right]} = \frac{K_3}{K_2} \times \frac{1}{\left(\gamma_{Ca^{2+}}\left[Ca^{2+}\right]\right)\gamma_{CaUO_2(CO_3)_3^{2-}}} \tag{13a}$$

Thus, the fraction of $CaUO_2(CO_3)_3^{2-}$ will be

$$f_{CaUO_2(CO_3)_3^{2-}} = \left(\frac{K_3}{K_2} \times \frac{1}{\gamma_{CaUO_2(CO_3)_3^{2-}} \left(\gamma_{Ca^{2+}} \left[Ca^{2+} \right] \right)} \right) \times f_{neutral} \quad (16)$$

In the same way, the fraction of $MgUO_2(CO_3)_3^{2-}$ will be

$$f_{MgUO_2(CO_3)_3^{2-}} = \left(\frac{K_4}{K_2} \times \frac{\left(\gamma_{Mg^{2+}} \left[Mg^{2+} \right] \right)}{\gamma_{MgUO_2(CO_3)_3^{2-}} \left(\gamma_{Ca^{2+}} \left[Ca^{2+} \right] \right)^2} \right) \times f_{neutral} \quad (17)$$

Because the total fraction of the four U species is 1, we can get equation (20) below.

$$\begin{aligned} 1 &= f_{neutral} + f_{UO_2(CO_3)_3^{4-}} + f_{CaUO_2(CO_3)_3^{2-}} + f_{MgUO_2(CO_3)_3^{2-}} \\ &= f_{neutral} + \left(\frac{K_1}{K_2} \times \frac{1}{\gamma_{UO_2(CO_3)_3^{4-}} \left(\gamma_{Ca^{2+}} \left[Ca^{2+} \right] \right)^2} \right) \times f_{neutral} + \left(\frac{K_3}{K_2} \times \frac{1}{\left(\gamma_{Ca^{2+}} \left[Ca^{2+} \right] \right) \gamma_{CaUO_2(CO_3)_3^{2-}}} \right) \times f_{neutral} \\ &\quad + \left(\frac{K_4}{K_2} \times \frac{\left(\gamma_{Mg^{2+}} \left[Mg^{2+} \right] \right)}{\left(\gamma_{Ca^{2+}} \left[Ca^{2+} \right] \right)^2 \gamma_{MgUO_2(CO_3)_3^{2-}}} \right) \times f_{neutral} \\ &= \left(1 + \frac{K_1}{K_2} \times \frac{1}{\gamma_{UO_2(CO_3)_3^{4-}} \left(\gamma_{Ca^{2+}} \left[Ca^{2+} \right] \right)^2} + \frac{K_3}{K_2} \times \frac{1}{\left(\gamma_{Ca^{2+}} \left[Ca^{2+} \right] \right) \gamma_{CaUO_2(CO_3)_3^{2-}}} + \frac{K_4}{K_2} \times \frac{\left(\gamma_{Mg^{2+}} \left[Mg^{2+} \right] \right)}{\left(\gamma_{Ca^{2+}} \left[Ca^{2+} \right] \right)^2 \gamma_{MgUO_2(CO_3)_3^{2-}}} \right) \times f_{neutral} \end{aligned} \quad (20)$$

APPENDIX B

U ISOTOPIC DATA

The last sample in all these tables are U in the bulk solid. In Table 9, samples C 3-1-1 to C 3-1-7 are daily solid samples. All the others are aqueous samples. U concentration in $CaCO_3$ is expressed as $U/CaCO_3$ (ppm).

Table 4. U isotopic compositions in aragonite experiment A_1 at pH 8.50 ± 0.10

Sample No.	U(ppm)	$\delta^{238}U$(‰)	2 SD(‰)
A 1-0	11.00	-0.22	0.10
A 1-1	9.15	-0.24	0.10
A 1-2	7.35	-0.23	0.05
A 1-3	5.90	-0.25	0.09
A 1-4	4.79	-0.25	0.04
A 1-5	3.82	-0.25	0.10
A 1-6	2.99	-0.34	0.03
A 1-7	2.35	-0.30	0.08
A 1-8	1.79	-0.35	0.03
A 1-9	1.34	-0.30	0.07
A 1-10	0.99	-0.39	0.08
A 1-11	0.71	-0.39	0.10
A 1-12	0.49	-0.44	0.05
A 1-13	0.30	-0.44	0.05
A 1-BS	2145	-0.24	0.08

Table 5. U isotopic compositions in aragonite experiment A_2 at pH 7.50 ± 0.10

Sample No.	U(ppm)	$\delta^{238}U$(‰)	2 SD(‰)
A 2-0	10.90	-0.25	0.01
A 2-1	10.61	-0.26	0.10
A 2-2	5.30	-0.26	0.10
A 2-3	1.86	-0.24	0.09
A 2-4	0.32	-0.29	0.09
A 2-5	0.08	-0.36	0.09
A 2-6	0.03	-0.35	0.10
A 2-7	0.02	-0.28	0.09
A 2-BS	2525	-0.30	0.05

Table 6. U isotopic compositions in aragonite experiment A_1* at pH 8.50 ± 0.10

Sample No.	U(ppm)	δ^{238}U(‰)	2 SD(‰)
A* 1-0	10.71	-0.23	0.01
A* 1-1	10.75	-0.27	0.02
A* 1-2	8.16	-0.24	0.04
A* 1-3	6.08	-0.27	0.01
A* 1-4	4.76	-0.28	0.08
A* 1-5	3.25	-0.29	0.07
A* 1-6	2.38	-0.30	0.05
A* 1-7	1.79	-0.29	0.10
A* 1-8	1.19	-0.36	0.05
A* 1-9	0.77	-0.33	0.10
A* 1-10	0.53	-0.34	0.07
A* 1-11	0.42	-0.37	0.08
A* 1-12	0.41	-0.38	0.08
A* 1-13	0.29	-0.37	0.05
A* 1-BS	2053	-0.23	0.02

Table 7. U isotopic compositions in aragonite experiment A_3 at pH 8.50 ± 0.10

Sample No.	U(ppm)	δ^{238}U(‰)	2 SD(‰)
A 3-0	10.17	-0.22	0.01
A 3-1	9.98	-0.21	0.05
A 3-2	5.52	-0.22	0.04
A 3-3	3.36	-0.25	0.08
A 3-4	1.96	-0.22	0.04
A 3-5	0.81	-0.28	0.03
A 3-6	0.42	-0.30	0.06
A 3-7	0.21	-0.33	0.08
A 3-8	0.01	-0.35	0.08
A 3-BS	2075	-0.26	0.08

Table 8. U isotopic compositions in aragonite experiment C_1 at pH 8.50 ± 0.10

Sample No.	U(ppm)	$\delta^{238}U$(‰)	2 SD(‰)
C 1-0	11.18	-0.23	0.05
C 1-1	10.93	-0.27	0.06
C 1-2	10.71	-0.25	0.05
C 1-3	10.47	-0.30	0.07
C 1-4	10.25	-0.25	0.06
C 1-5	9.86	-0.21	0.10
C 1-6	9.72	-0.27	0.07
C 1-7	9.56	-0.24	0.07
C 1-8	9.34	-0.25	0.04
C 1-9	9.02	-0.23	0.05
C 1-10	9.01	-0.20	0.04
C 1-11	8.68	-0.21	0.04
C 1-12	8.50	-0.23	0.09
C 1-13	8.14	-0.22	0.02
C 1-BS	336	-0.33	0.09

Table 9. U isotopic compositions in aragonite experiment C_2 at pH 7.50 ± 0.10

Sample No.	U(ppm)	$\delta^{238}U$(‰)	2 SD(‰)
C 2-0	11.18	-0.22	0.00
C 2-1	9.60	-0.22	0.07
C 2-2	8.83	-0.24	0.10
C 2-3	8.94	-0.27	0.02
C 2-4	8.91	-0.27	0.04
C 2-5	9.14	-0.23	0.07
C 2-6	8.93	-0.20	0.08
C 2-7	8.51	-0.21	0.03
C 2-BS	360	-0.21	0.04

Table 10. U isotopic compositions in aragonite experiment C_3 at pH 8.50 ± 0.10

Sample No.	U(ppm)	$\delta^{238}U$(‰)	2 SD(‰)
C 3-0	10.60	-0.22	0.04
C 3-1	5.78	-0.25	0.06
C 3-2	4.75	-0.20	0.05
C 3-3	3.56	-0.20	0.03
C 3-4	3	-0.25	0.07
C 3-5	2.41	-0.20	0.06
C 3-6	2.04	-0.22	0.04
C 3-7	1.68	-0.22	0.05
C 3-8	1.37	-0.30	0.07
C 3-9	1.13	-0.25	0.07
C 3-10	0.89	-0.20	0.05
C 3-11	0.7	-0.17	0.09
C 3-12	0.58	-0.17	0.08
C 3-13	0.49	-0.24	0.04
C 3-1-1	6.38	-0.18	0.04
C 3-1-2	20.63	-0.22	0.07
C 3-1-3	16.25	-0.29	0.10
C 3-1-4	4.05	-0.20	0.04
C 3-1-5	3.73	-0.21	0.10
C 3-1-6	0.23	-0.31	0.10
C 3-1-7	2.45	-0.17	0.06
C 3-BS	250	-0.22	0.05

APPENDIX C

UNCERTAINTIES IN RAYLEIGH FRACTIONATION FACTOR

The uncertainties of Rayleigh isotopic fractionation factors are estimated using a two-error York regression of equation (3) with ISOPLOT 3.75.

$$\ln\left(\delta^{238}U_{solution}+1000\right)=(\alpha-1)\ln f+\ln\left(\delta^{238}U_0+1000\right) \quad (3)$$

Here are results of the linear regression of equation (3) in each experiment.

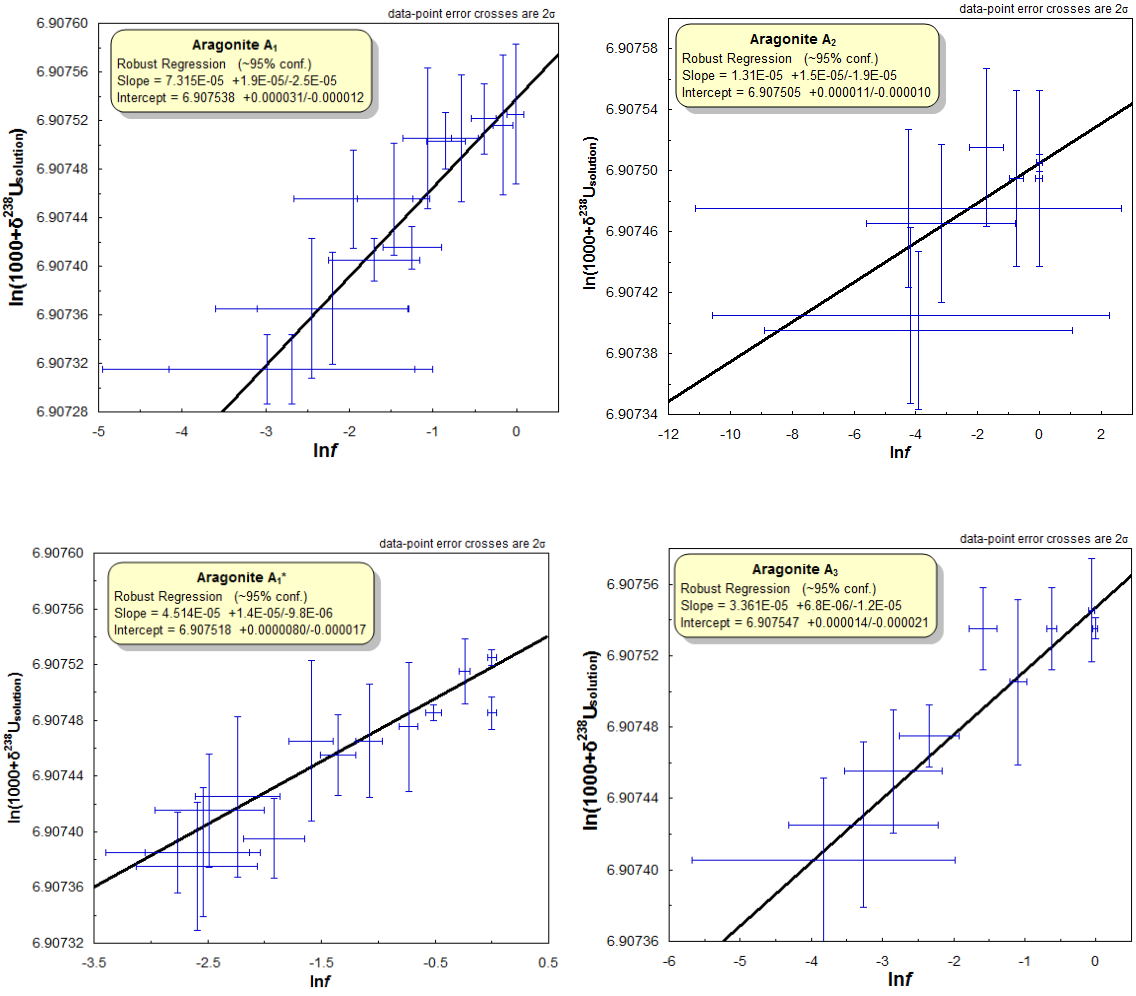

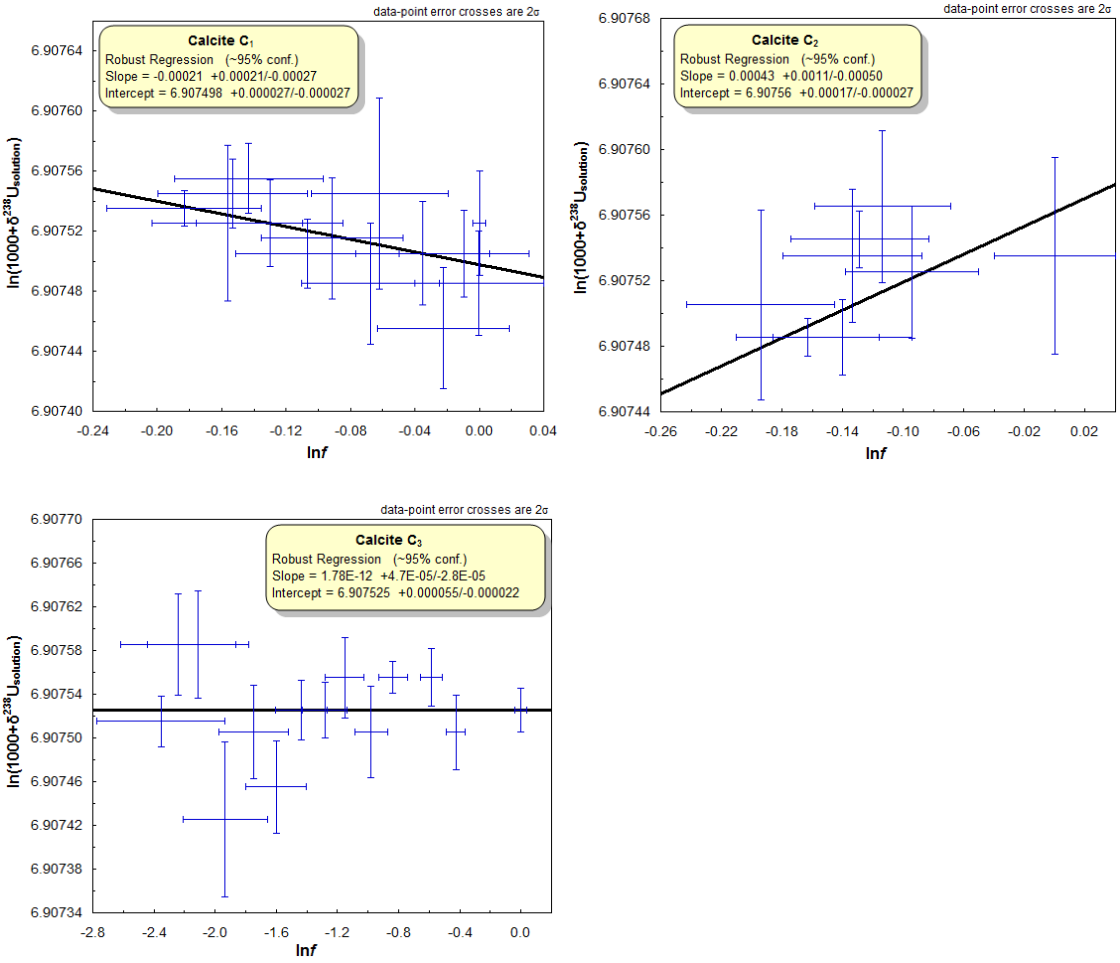

Fig. 9 Estimation of the Rayleigh isotopic fractionation factors and their uncertainties in calcium carbonate coprecipitation experiments.